We are IntechOpen,
the world's leading publisher of
Open Access books
Built by scientists, for scientists

4,800
Open access books available

122,000
International authors and editors

135M
Downloads

Our authors are among the

154
Countries delivered to

TOP 1%
most cited scientists

12.2%
Contributors from top 500 universities

BOOK CITATION INDEX — CLARIVATE ANALYTICS — INDEXED

WEB OF SCIENCE™

Selection of our books indexed in the Book Citation Index
in Web of Science™ Core Collection (BKCI)

Interested in publishing with us?
Contact book.department@intechopen.com

Numbers displayed above are based on latest data collected.
For more information visit www.intechopen.com

Faults Detection for Power Systems

Zeng Xiangjun,Wang Yuanyuan and Xu Yao
Changsha University of Science and Technology
China

1. Introduction

Power systems are the largest and most complex human made systems, where faults always occurred, in the world. Faults can cause personnel and equipment safety problems, and can result in substantial economic losses. In order to solve the problems, faults automatic detection, location and isolation must be employed. Most faults can cause large currents or voltages changing, and they are often detected by traditional protective relay. Whereas, some faults, such as high impedance faults, grounding faults of ineffectively earthed distribution systems, cause small currents and voltages changing and they are difficult to be detect using traditional protective relay. In this chapter, faults generated signals characteristics are investigated, special faults detection methods are developed, and their applications in power systems are presented.

2. Faults generated signals characteristics

2.1 Fundamental frequency signals characteristics

The three phase voltages and currents include fundamental frequency signals and many other different frequency harmonic signals. In this section the fundamental frequency signals is analyzed (Jingchao et al. 2003, Yang et al. 2003, Wang et al. 2006).
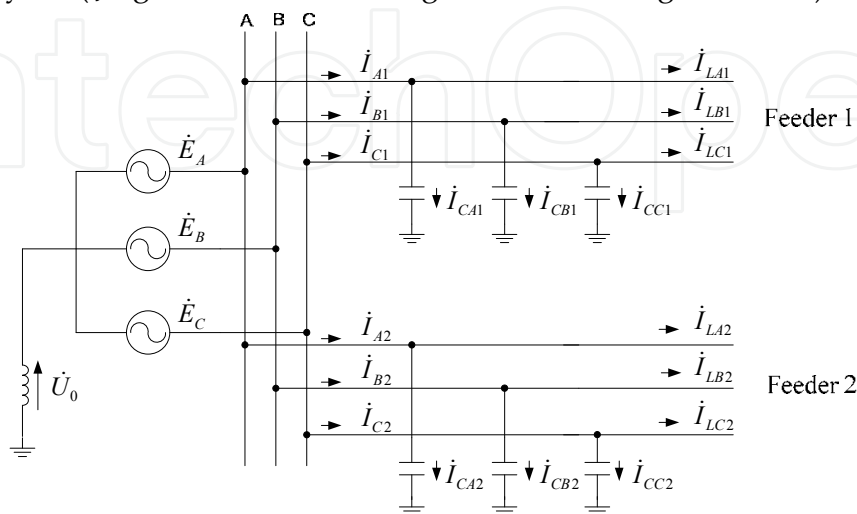

Fig. 1. Current direction of ineffectively earthed distribution system in normal condition

A typical ineffectively earthed distribution system is shown in Figure 1. The three phase fundamental frequency voltages named $\dot{E}_A$, $\dot{E}_B$ and $\dot{E}_C$ and fundamental frequency currents are symmetrical in normal condition. The neutral-to-ground voltage $\dot{U}_0$ is zero, and the phase-to-ground capacitances in Feeder 1 and Feeder 2 are C_1 and C_2 respectively. Taking Feeder 1 for example, the three phase fundamental frequency currents flowing from bus to feeder are $\dot{I}_{A1}$, $\dot{I}_{B1}$, $\dot{I}_{C1}$, the fundamental frequency capacitive currents are $\dot{I}_{CA1}$, $\dot{I}_{CB1}$, $\dot{I}_{CC1}$, and fundamental frequency load currents are $\dot{I}_{LA1}$, $\dot{I}_{LB1}$, $\dot{I}_{LC1}$.

The three phase fundamental frequency currents from bus to Feeder 1 can be calculated:

$$\begin{cases} \dot{I}_{A1} = \dot{I}_{CA1} + \dot{I}_{LA1} = j\omega C_1(\dot{E}_A + \dot{U}_0) + \dot{I}_{LA1} \\ \dot{I}_{B1} = \dot{I}_{CB1} + \dot{I}_{LB1} = j\omega C_1(\dot{E}_B + \dot{U}_0) + \dot{I}_{LB1} \\ \dot{I}_{C1} = \dot{I}_{CC1} + \dot{I}_{LC1} = j\omega C_1(\dot{E}_C + \dot{U}_0) + \dot{I}_{LC1} \end{cases} \tag{1}$$

The three phase fundamental frequency currents from bus to Feeder 2 can be calculated:

$$\begin{cases} \dot{I}_{A2} = \dot{I}_{CA2} + \dot{I}_{LA2} = j\omega C_2(\dot{E}_A + \dot{U}_0) + \dot{I}_{LA2} \\ \dot{I}_{B2} = \dot{I}_{CB2} + \dot{I}_{LB2} = j\omega C_2(\dot{E}_B + \dot{U}_0) + \dot{I}_{LB2} \\ \dot{I}_{C2} = \dot{I}_{CC2} + \dot{I}_{LC2} = j\omega C_2(\dot{E}_C + \dot{U}_0) + \dot{I}_{LC2} \end{cases} \tag{2}$$

If single-phase grounding fault happened in phase C of Feeder 2 (shown in Figure 2), the three phase fundamental frequency voltages of source are still symmetrical. But the neutral-to-ground voltage is not zero, it changes from $\dot{U}_0$ to $\dot{U}_0'$. The residual current is $\dot{I}_f$.

Taking Feeder 1 for example, the three phase fundamental frequency currents are $\dot{I}_{A1}'$, $\dot{I}_{B1}'$ and $\dot{I}_{C1}'$ respectively, fundamental frequency capacitive currents are $\dot{I}_{CA1}'$, $\dot{I}_{CB1}'$ and $\dot{I}_{CC1}'$ respectively, and fundamental frequency load currents are $\dot{I}_{LA1}'$, $\dot{I}_{LB1}'$ and $\dot{I}_{LC1}'$ respectively.
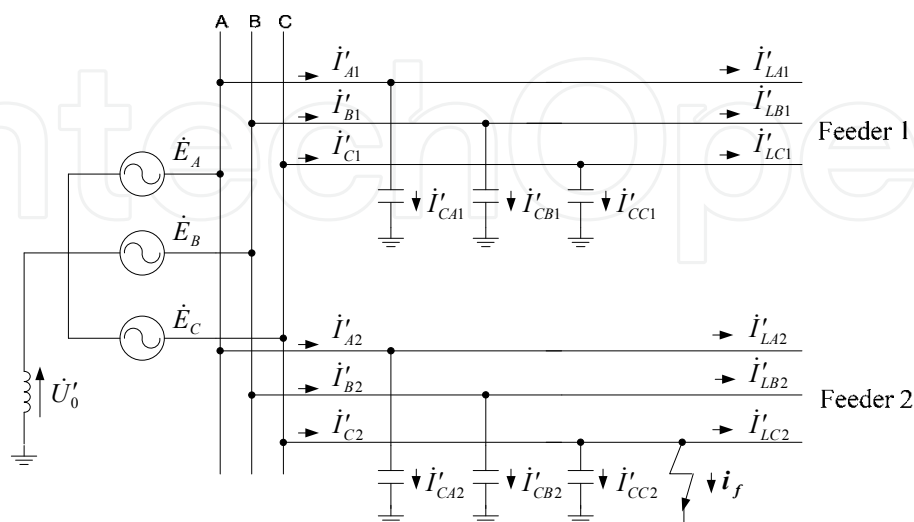

Fig. 2. Current direction of ineffectively earthed distribution system when single-phase grounding fault happened

The three phase fundamental frequency currents from bus to Feeder 1 can be calculated:

$$\begin{cases} \dot{I}'_{A1} = \dot{I}'_{CA1} + \dot{I}'_{LA1} = j\omega C_1(\dot{E}_A + \dot{U}'_0) + \dot{I}'_{LA1} \\ \dot{I}'_{B1} = \dot{I}'_{CB1} + \dot{I}'_{LB1} = j\omega C_1(\dot{E}_B + \dot{U}'_0) + \dot{I}'_{LB1} \\ \dot{I}'_{C1} = \dot{I}'_{CC1} + \dot{I}'_{LC1} = j\omega C_1(\dot{E}_C + \dot{U}'_0) + \dot{I}'_{LC1} \end{cases} \quad (3)$$

The three phase fundamental frequency currents from bus to Feeder 2 can be calculated:

$$\begin{cases} \dot{I}'_{A2} = \dot{I}'_{CA2} + \dot{I}'_{LA2} = j\omega C_2(\dot{E}_A + \dot{U}'_0) + \dot{I}'_{LA2} \\ \dot{I}'_{B2} = \dot{I}'_{CB2} + \dot{I}'_{LB2} = j\omega C_2(\dot{E}_B + \dot{U}'_0) + \dot{I}'_{LB2} \\ \dot{I}'_{C2} = \dot{I}'_{CC2} + \dot{I}'_{LC2} + \dot{I}_f = j\omega C_2(\dot{E}_C + \dot{U}'_0) + \dot{I}'_{LC2} + \dot{I}_f \end{cases} \quad (4)$$

Although the three phase fundamental frequency currents contain fundamental frequency load currents, the fundamental frequency load currents change little before and after fault happening. It can be assumed:

$$\begin{cases} \dot{I}_{LA1} = \dot{I}'_{LA1}, \dot{I}_{LA2} = \dot{I}'_{LA2} \\ \dot{I}_{LB1} = \dot{I}'_{LB1}, \dot{I}_{LB2} = \dot{I}'_{LB2} \\ \dot{I}_{LC1} = \dot{I}'_{LC1}, \dot{I}_{LC2} = \dot{I}'_{LC2} \end{cases} \quad (5)$$

Comparing (1), (2), (3), (4) and taking account of (5), the changing of the fundamental frequency currents can be calculated.
For Feeder 1:

$$\begin{cases} \Delta \dot{I}_{A1} = \dot{I}'_{A1} - \dot{I}_{A1} = j\omega C_1(\dot{U}'_0 - \dot{U}_0) \\ \Delta \dot{I}_{B1} = \dot{I}'_{B1} - \dot{I}_{B1} = j\omega C_1(\dot{U}'_0 - \dot{U}_0) \\ \Delta \dot{I}_{C1} = \dot{I}'_{C1} - \dot{I}_{C1} = j\omega C_1(\dot{U}'_0 - \dot{U}_0) \end{cases} \quad (6)$$

For Feeder 2:

$$\begin{cases} \Delta \dot{I}_{A2} = \dot{I}'_{A2} - \dot{I}_{A2} = j\omega C_2(\dot{U}'_0 - \dot{U}_0) \\ \Delta \dot{I}_{B2} = \dot{I}'_{B2} - \dot{I}_{B2} = j\omega C_2(\dot{U}'_0 - \dot{U}_0) \\ \Delta \dot{I}_{C2} = \dot{I}'_{C2} - \dot{I}_{C2} = j\omega C_2(\dot{U}'_0 - \dot{U}_0) + \dot{I}_f \end{cases} \quad (7)$$

The differences of the changing of the fundamental frequency currents of Feeder 1 between the phases can be calculated as:

$$\begin{cases} \Delta \dot{I}_{AB1} = \Delta \dot{I}_{A1} - \Delta \dot{I}_{B1} = 0 \\ \Delta \dot{I}_{BC1} = \Delta \dot{I}_{B1} - \Delta \dot{I}_{C1} = 0 \\ \Delta \dot{I}_{CA1} = \Delta \dot{I}_{C1} - \Delta \dot{I}_{A1} = 0 \end{cases} \quad (8)$$

For Feeder 2:

$$\begin{cases} \Delta\dot{I}_{AB2} = \Delta\dot{I}_{A2} - \Delta\dot{I}_{B2} = 0 \\ \Delta\dot{I}_{BC2} = \Delta\dot{I}_{B2} - \Delta\dot{I}_{C2} = -\dot{I}_f \\ \Delta\dot{I}_{CA2} = \Delta\dot{I}_{C2} - \Delta\dot{I}_{A2} = \dot{I}_f \end{cases} \qquad (9)$$

From the above analysis, the following results are obtained:

a.   In the sound feeder, the differences of the changing of the fundamental frequency currents between the three phases are zero under the ideal conditions.

b.   In the faulted feeder, the differences of the changing of the fundamental frequency currents between the healthy and faulted phases are very large, equaling the residual current. However, it is zero between healthy phase currents.

In order to reduce the measuring error and the unbalance effect, the changing of the fundamental frequency currents ($\Delta\dot{I}$) is applied, which can be calculated by the following methods(Zeng et al. 2001):

a. $i(n) = i(n) - i(n-T)$

b. $i(n) = i(n) + i(n-T/2)$

c. $i(n) = i(n) - 2i(n-T) + i(n-2T)$

d. $i(n) = i(n) + i(n-T/2) - i(n-T) - i(n-3T/2)$

Where, n is the sample-time in digital relay, T is the system period (20ms when system frequency is 50Hz). Among the above methods, method d is usually employed.

2.2 Transient signals characteristics

2.2.1 High frequency characteristics

High frequency transient has high propagation velocity, and a large extent of attenuation, which lead to distortion on the process of transmission along the line. The transmission characteristics of different frequency components will result in the distortion of traveling waves, and the phenomenon is called dispersion, which decreases the mutation of initial traveling wave, influences the effective identification of initial traveling wave.

By analyzing the modulus of the frequency characteristics of the parameters, earth simulator component has the most serious attenuation and phase shift in the process of transmission, in that the earth simulator component is seriously influenced by zero-order inductance and resistance. The zero-order inductance and resistance is closely related with frequency because of skin effect. With obviously decreased of frequency, the zero-order inductance is decreased, while the zero-order resistance is increased, which cause attenuation coefficient and wave velocity have great changes. The higher frequency is included in earth simulator component, the more serious attenuation generated during transmission. Line model has greatly influenced by zero-order inductance and resistance, but these parameters have smaller impact of frequency. So attenuation coefficient and wave velocity of Line model are far less impact to earth simulator component. Therefore, dispersion of traveling wave is mainly caused by earth simulator component.

Seen from the fault type, single-phase grounding will generate large quantity of earth simulator component, which is greatly influenced by dispersion; two-phase earth short circuit has weak earth simulator component, which has smaller dispersion; two or

three-phase short circuit has minimal impact, which has the smallest dispersion.

In practical application, the frequency band range of traveling wave is valued between 10 kHz to 1MHz. In this range, line model of traveling wave velocity has little influence by frequency changes, which has limited impacts for fault location. While high frequency component is serious attenuated, which to some extend decreased the amplitude of initial traveling wave.

Frequency characteristics of each modulus parameters, frequency variation curve of modulus velocity and frequency variation curve of modulus wave impedance are shown in Figure 3, 4 and 5 (Guo. 2007).
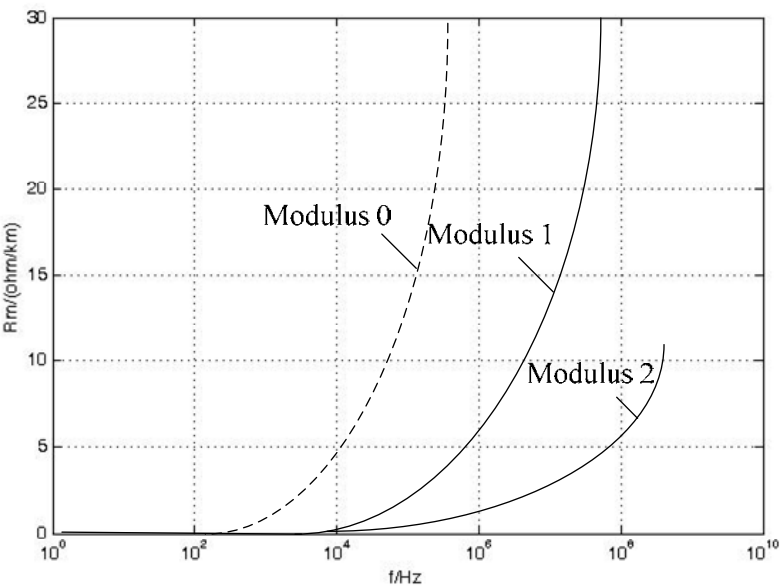
(a) Resistance frequency dependent character of each modulus parameters
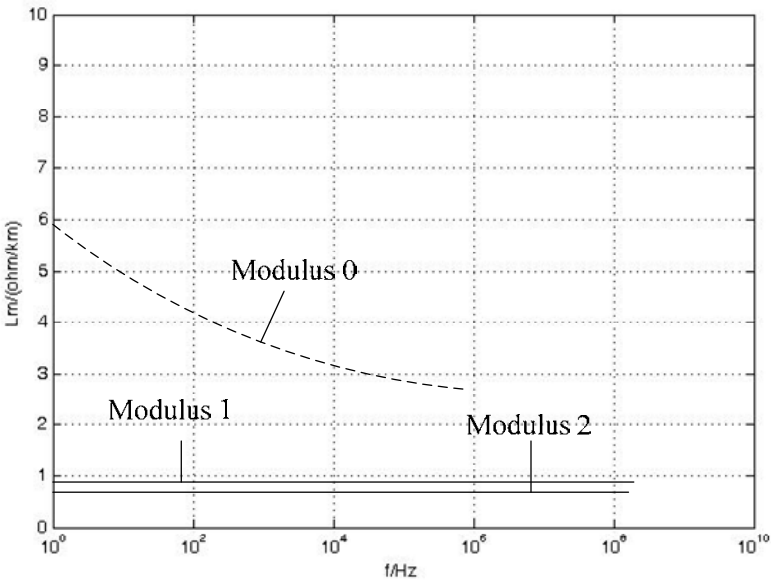
(b) Inductance frequency dependent character of each modulus parameters

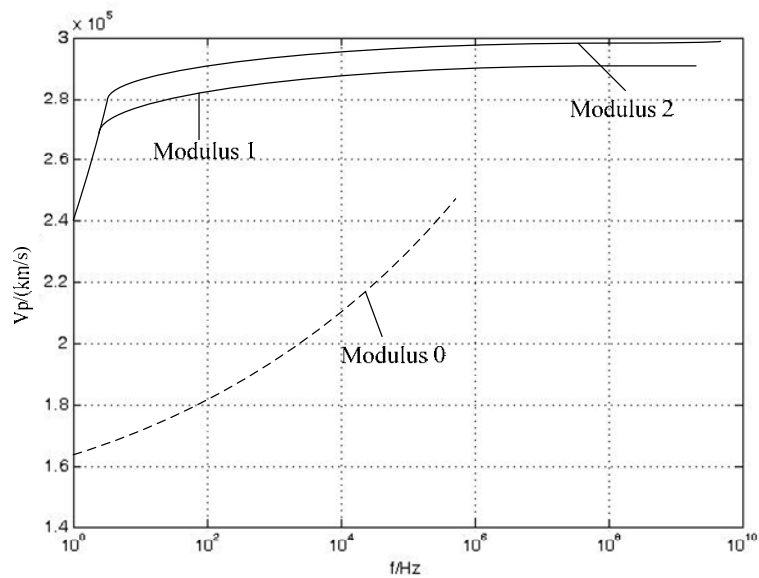Fig. 3. Frequency characteristics of each modulus parameters

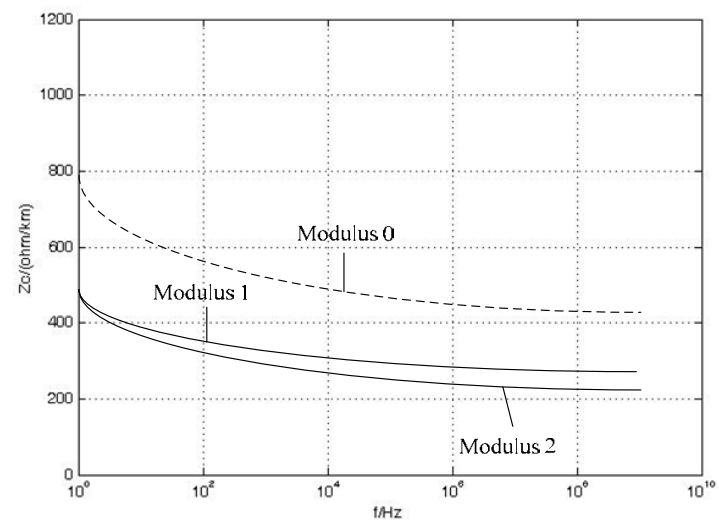Fig. 4. Frequency variation curve of modulus velocity

Fig. 5. Frequency variation curve of modulus wave impedance

2.2.2 Transient signals analysis with fourier transform

A signal $x(t)$ can be represented in the form(Wang et al. 2002):

$$x(t) = \int_{-\infty}^{\infty} F(\omega)e^{j\omega t}d\omega \tag{10}$$

Where $F(\omega)$, the Fourier transform of $x(t)$, is defined as:

$$\hat{x}(\omega) = \frac{1}{2\pi}\int_{-\infty}^{\infty} x(t)e^{-j\omega t}dt \tag{11}$$

The Fourier transform $\hat{x}(\omega)$ depend on the global properties of $x(t)$.

Short time Fourier transform (STFT) is the Fourier transform of signal $x(t)$ multiplied by a window function translating in time by b:

$$STFT(\omega, b) = \int_{-\infty}^{\infty} x(t)\overline{w}(t-b)e^{-j\omega t}dt \tag{12}$$

Where $\overline{w}$ denotes the conjugate of window function w. It can be rewritten as:

$$STFT_x(\omega, b) = e^{-jwb} \int_{-\infty}^{\infty} x(t)\overline{w}(-(b-t))e^{j\omega(b-t)}dt \tag{13}$$

Therefore, short time Fourier transform of a signal is that the signal is firstly through a band pass filter at analyzing frequency ω and then is modulated to zero frequency.

2.2.3 Transient signals analysis with wavelet transform

Proper signal analysis becomes a key issue. Analyzing singly in the time or frequency domain is not sufficient to capture the faults that spread in a wide band of frequencies. Faults of these types require analysis which is localized in both the time and frequency domains. The wavelet transform is an excellent signal analysis and decomposition tool for such signals using constant bandwidth analysis.

A Function $\Psi(t) \in L^2(R)$ is called a basic wavelet or mother wavelet, if the Fourier Transform satisfies equation (14) (Zhang et al. 2004):

$$\int_{-\infty}^{\infty} \frac{\left|\psi^*(\omega)\right|^2}{|\omega|}d\omega < \infty \tag{14}$$

Where $\psi^*(\omega)$ is the Fourier Transform of function $\psi(\omega)$. With its dilation and translation, we can get equation (15):

$$\psi_{a,b}(t) = \frac{1}{\sqrt{|a|}}\psi(\frac{t-b}{a}), b \in R, a > 0 \tag{15}$$

This is called continuous wavelet relaying on factors a and b. Where a is called dilation factor and b is called translation factor. The continuous wavelet translation of a function $f(t) \in L^2(R)$ will be equation (16):

$$W_f(a,b) = <f, \psi_{a,b}> = |a|^{\frac{1}{2}} \int_R f(t)\psi(\frac{t-b}{a})dadb \tag{16}$$

The function can be restructured by equation (17):

$$f(t) = \frac{1}{C_\psi} \int_{-\infty}^{\infty} \int_{-\infty}^{\infty} \frac{1}{a^2} W_f(a,b)\psi(\frac{t-b}{a})dadb \tag{17}$$

Continuous wavelet transform (CWT) has perfect localization both in time domain and in frequency domain. With $|a|$ decrease, $\psi_{a,b}(t)$ focuses on the part of high frequency. It means the narrow in time window but high resolution. This performance makes CWT an advanced tool on fault detection.

When used in practice cases, especially in implementation in computer, continuous wavelet has been discrete. In fact, continuous wavelet and continuous wavelet transform of a signal can both be discrete. Supposing $a = a_0^j$ and $b = ka_0^j b_0$ $j \in Z$, equation (18):

$$\psi_{j,k}(t) = a_0^{-j/2}\psi(a_0^{-j}t - kb_0) \qquad (18)$$

The decomposition and its reconstruction of the function $f(t)$ in discrete wavelet transform are shown in equation (19) and (20):

$$C_{j,k} = < f, \psi_{j,k} > = \int_{-\infty}^{\infty} f(t)\psi_{j,k}(t)dt \qquad (19)$$

$$f(t) = C\sum_{-\infty}^{\infty}\sum_{-\infty}^{\infty} C_{j,k}\psi_{j,k}(t) \qquad (20)$$

Different wavelet transform may give different analysis results to the system. To most vibration signal, both CWT and discrete wavelet transform (DWT) can be used to detect faults.

There is a significant difference between wavelet transform and Fourier transform. The Fourier based functions are indexed by a single frequency parameter ω whereas the wavelet ones are indexed by two parameters, scale a and time translation b. Therefore, Fourier transforms describe the global properties of $x(t)$ while wavelet transforms describe the local properties of $x(t)$ in the neighborhood of each time translation b.

Short Time Fourier transform, which is the function of two variables: time translation b and analyzing frequency ω, shares with wavelet transform the same property of localization. It is customary to think of short time Fourier transform as the frequency analysis of a signal in a short time, particularly in the case of rectangular window, but the short time Fourier transform of signal $x(t)$ depends not only on the signal but also on the choice of the window.

2.2.4 Transient signals analysis with Hilbert transform

When we have decomposed the signal into a series of IMFS, Hilbert transform can be carried out on each intrinsic mode function (IMF) to get a series of instantaneous frequency $f_i(t)$ (Xiao'an et al. 2008).

For each IMF $c_i(t)$, its corresponding Hilbert transform is defined as:

$$Y_i(t) = \frac{1}{\pi}\int_{-\infty}^{+\infty}\frac{c_i(\tau)}{t-\tau}d\tau \qquad (21)$$

Thus an analytic signal $Z_i(t)$ can be constructed as:

$$Z_i(t) = c_i(t) + jY_i(t) = a(t)e^{i\theta(t)} \qquad (22)$$

Where $a(t) = [c_i(t)^2 + Y_i(t)^2]^{\frac{1}{2}}$; $\theta(t) = \arctan(Y_i(t)/c_i(t))$.

Instantaneous frequency of $c_i(t)$ is defined as:

$$f(t) = \frac{1}{2\pi}\frac{d\theta(t)}{dt} \qquad (23)$$

2.2.5 Transient signals analysis with Hilbert-Huang transform

Hilbert-Huang Transform (HHT) is used for analyzing non-stationary and nonlinear signal. Compared with Fourier transform and wavelet transform, it is not necessary to select parameters in HHT, and the results of HHT absolutely lie only on the character of the signal itself. The transform has only one result.

HHT is based on two processes: empirical mode decomposition (EMD) and Hilbert transform. The central part of the HHT is EMD which is a sifting process to decompose a signal into a number of IMFs. Each IMF must satisfy the following two conditions: a) In the whole data set, the number of extrema and the number of zero-crossings must either equal or differ at most by one; b) At any point, the mean value of the envelope defined by local maxima and the envelope defined by the local minima is zero.

Any signal $s(t)$ can be decomposed as follows (Xiao'an et al. 2008):

a. When $s_{11}(t) = s(t)$, subscript i of signal $s_{ij}(t)$ expresses the decomposing order, and subscript j expresses the sifting times in the i order. Find all the local extrema, including maxima and minima, then connect all the maxima and minima of signal $s(t)$ using smooth cubic splines to get its upper envelope and lower envelope.

b. Subtracting mean $m_{ij}(t)$ of these two envelopes from the signal $s_{ij}(t)$ to get their difference: $h_{ij}(t) = s_{ij}(t) - m_{ij}(t)$.

c. If the sifting result $h_{ij}(t)$ meets the two criteria of an IMF, carry out step d; otherwise, treat $s_{i(j+1)}(t) = h_{ij}(t)$, and repeat steps a and b.

d. The i th IMF of signal $s(t)$ is: $c_i(t) = h_{ij}(t)$. Calculate the residual signal: $r_i(t) = s_{i1}(t) - c_i(t)$.

e. If the residue becomes monotonic, the final order $n = i$; Otherwise, treat $s_{(i+1)1}(t) = r_i(t)$, repeat steps a, b, c and d.

The original signal $s(t)$ can thus be expressed as follows:

$$s(t) = \sum_{i=1}^{n} c_i(t) + r_n(t) \tag{24}$$

Where $c_i(t)$ is i th IMF component, and $r_n(t)$ is the residue.

In summary, the empirical mode decomposition is similar with wavelet decomposition. The tree of empirical mode decomposition is shown in Figure 6. For the first IMF $c_1(t)$ contains the highest frequency component of the signal, it can be applied to fault detection (Li. 2005).
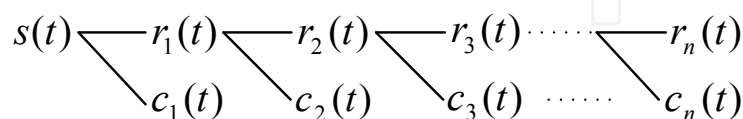
$$s(t) \diagdown r_1(t) \diagdown r_2(t) \diagdown r_3(t) \cdots \diagdown r_n(t)$$
$$\diagdown c_1(t) \quad \diagdown c_2(t) \quad \diagdown c_3(t) \quad \cdots \diagdown c_n(t)$$

Fig. 6. Tree of empirical mode decomposition

2.3 Sensors and their characteristics analysis

Predicting or locating the faults as soon as possible is very important to maintain power grid reliable operation. Moreover, faults often accompanied by ultrasonic, electromagnetic field distribution and temperature changing, etc. Based on the change of these physical

parameters, faults can locate quickly and accurately, so that the repair work can be carried out in the minimum time.

2.3.1 Sensors for faults generated ultrasonic

The basic idea of ultrasonic sensors is quite simple: They transmit acoustic waves and receive them after interaction of ultrasonic wave and investigated process. On it's arrival at the receiver the ultrasound signal carries the information about the parameters to be measured (and unfortunately many other parameters too – which demands compensation). In addition, software algorithms based on models for the ultrasonic propagation and the interaction between the ultrasonic wave and physical or chemical variables of interest are employed for analysis the measuring. Furthermore, ultrasonic measurements are only meaningful when state parameters like temperature, pressure etc. are measured simultaneously with the ultrasonic parameters at high accuracy for compensation.

Ultrasound covers a frequency range from 20 kHz to about 1 GHz. For technical applications the range 20 kHz to 10 MHz is the most important one (Hauptmann et al. 2001). The attractive features of ultrasonic sensors can be summarized as follow:

a.   Non-invasive measurement.
b.   In-line measurement.
c.   Rapid response, usually a fraction of a second.
d.   Low power consumption.
e.   Excellent long term stability.
f.   High resolution and accuracy.

At present, ultrasonic technique has been applied to the detection and location of discharges in liquid-immersed dielectric structures such as gaps, coil stacks, and reactors. However, in some cases it probably can be extended to solid structures, if higher frequencies are used, and also to gas-filled structures by using lower frequencies. It is applicable for almost any type of voltage testing. It does not interfere with normal current and voltage measurements, and indicates the presence and location of sparks and corona. In addition, it is relatively insensitive to external disturbances and is not influenced by the test piece capacitance. Therefore, it can serve as a valuable adjunct to other methods of discharge detection and measurement (Cooper et al. 1984).

The most challenging issues facing ultrasonic sensors are:

a.   The exact knowledge of the acoustic properties of the substances is necessary for most ultrasonic measurements.
b.   Substances under investigation must be acoustically transparent for transmission and some reflection techniques.
c.   Ultrasonic measurements are highly disturbed when gas bubbles in liquids are present.
d.   Ultrasonic signals tend to be complicated and need relatively complex signal processing.
e.   Only integral information along the entire sound path is delivered.
f.   Increase of the attenuation of sound with frequency.

It is known that corona and spark breakdowns produce both audible and ultrasonic pressure waves in the medium surrounding the discharge. The pressure waves have an intensity which is determined by the rate of energy release and the nature of the medium in which the discharge occurs. These pressure waves propagate radically outward in all directions, and generally contain a wide range of frequency components of up to several

hundred kilocycles in liquid. In gases, the higher frequencies rapidly are attenuated, leaving only vibrations in the audible sound range. However, in liquid and in some solids, the attenuation of the higher frequencies is not as severe, and the electric discharges will produce pressure variations which have rich ultrasonic components, as well as audible sound.

The ultrasonic partial discharges measurement technique consists of two types, namely the contact type and the non-contact type. The contact-type measurement method uses a direct contact between the sensor and the equipment measured; for common transformer, the ultrasonic sensor was mounted on the wall of transformer to detect the ultrasonic signal and corona noise. But for some special transformer, such as epoxy-resin transformer, its coil surface relies on epoxy resin to insulate it from the air; it will be more difficult to use the contact-type measurement method in the field before the said phenomenon is resolved. The non-contact type measurement, although with a less degree of sensitivity than that of the contact type, experiences no such shortcoming mentioned above.

The sound wave's per-unit area energy and acoustic pressure will decrease as the propagation distance increases. Due to the rather weak partial discharges signals, their propagation distance is not far in the air and is easily interfered by the environment; hence ultrasonic measurement devices must be placed as closely to the measured object as possible. We will position the ultrasonic device, at various angles, 1m away from the object to be measured. During the measurement, we adopt partial discharges ultrasonic measuring devices with measurement frequency ranging from 20 to 100 kHz. To achieve the goal of identification of type and magnitude of fault, we design a partial discharges ultrasonic signal retrieving and analyzing system to proceed signal analysis; the whole analysis flowchart is shown in Figure 7 (Chen et al. 2005).
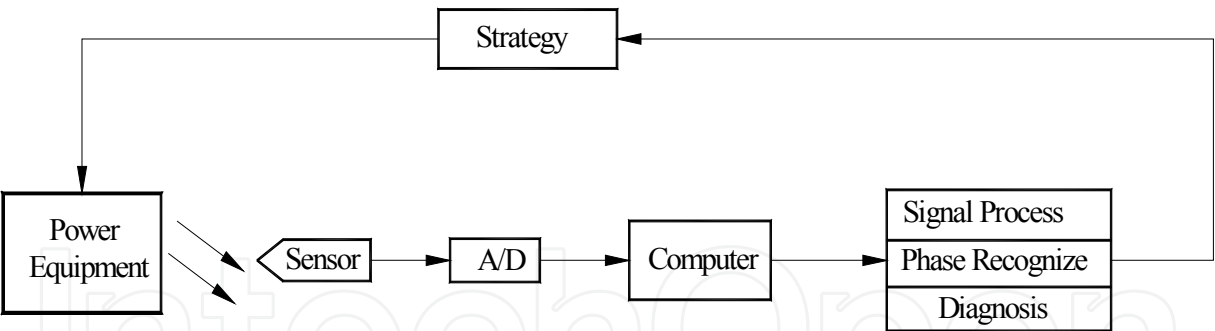

Fig. 7. Ultrasonic measurement flow

Step a.   Measuring ultrasonic signals and, after analog–digital conversion, filing them into computer and proceeding noise identification.

Step b.   Obtaining the field power-source signal as the reference signal; comparing ultrasonic signals with the reference signal to observe the discharges' sound wave characteristics.

Step c.   Using a 60 Hz signal's angle as the reference, draw partial discharges signals into 3-D diagrams with the angle, the period, and the magnitude as the coordinates to observe partial discharges angles' characteristics.

Step d.   Using a 60 Hz signal's angle as the reference; drawing partial discharges signals into polar-coordinate diagrams with the magnitude and the angle as the coordinates to observe partial discharges angles' characteristics.

Step e.   Draw zone-identification patterns and them with basic discharge patterns to determine the equipment's abnormal discharge type.

2.3.2 Sensors for faults generated electromagnetic field distribution

Electromagnetic Pulse (EMP) Measurements

The sensor factor is defined here as the time-domain relation between magnetic or electric field ($H(t)$ or $E(t)$) and the sensor output voltage $V(t)$ (Middelkoop 1991):

$$F_h(t) = H(t)/V(t) \quad [\text{A/m/V}], \text{ for a B-sensor} \tag{25}$$

$$F_e(t) = E(t)/\int_{\tau_i} V(t)dt \quad [\text{V/m/V}], \text{ for a } \overset{\circ}{D}\text{-sensor} \tag{26}$$

Where τ_i is an integration time constant, $F_h(t)$ and $F_e(t)$ represent the magnetic and electric sensor factors, respectively, $B = \mu \cdot H$ and $\overset{\circ}{D} = \delta E / \delta t$.

The sensor factor characterizes the sensitivity of the sensor to the field. It is the function of an equivalent surface or equivalent length of the sensor. For calibration purposes it is recommended that sensors with unambiguously calculable equivalent surfaces and lengths be used. The dipole antenna to measure the electric field when combined with an integrator and the short-circuited loop antenna to measure the magnetic field are suitable sensors.

Figure 8 (Middelkoop R. 1991) shows a relatively simple closed circular loop (CCL) magnetic field sensor for which the sensor factor is calculated. The current that is induced in the closed loop by a magnetic field is measured using a current transformer clamped onto the loop. It can be shown that the current in the loop equals

$$I(t) = \mu_0 A H(t) / L \tag{27}$$

Where $A = \pi(a-b)^2$ is the effective area, μ_0 is the free-space permeability ($\mu_0 = 4\pi \cdot 10^{-7} V \cdot s / A \cdot m$) and L is the inductance of the loop. If the loop width $2b$ is small compared to its radius a, $b^2 \ll a^2$ and small compared to the wavelength, then

$$L = A\mu_0 \{\ln(8a/b) - 2\} \tag{28}$$

The relation between the induced current $I(t)$ and the magnetic field $H(t)$ is therefore only dependent on the loop dimensions. In practice, however, a time-dependent response $R(t)$ is introduced by the current clamp. The insertion impedance of the clamp causes a low-frequency cutoff, commonly designated as "sensor droop." This droop influences in particular the late time response of the field sensor (in practice > 500ns). The effect can be corrected if the cutoff frequency is known. The sensor factor becomes

$$F_h(t) = \frac{a\{\ln(8a/b) - 2\}}{\pi R(t)(a-b)^2} \quad [\text{A/m/V}] \tag{29}$$

A hollow spherical dipole (HSD) sensor that acts as an electric field sensor is shown in Figure 9. (Middelkoop R. 1991). In this case one half of the dipole is replaced by a conducting

plane, so the sensor can be used asymmetrically, e.g., on the bottom plate of a TEM cell.
The current $I(t)$ is equal to the change in surface charge per unit of time of the sphere as a result of a time varying electric field perpendicular to the base plate. It can be shown that

$$I(t) = 3\pi r^2 \varepsilon_0 \frac{dE(t)}{dt} \tag{30}$$

Where r is the sphere radius and ε_0 the free-space permittivity ($\varepsilon_0 = 8.85 \cdot 10^{-12} A \cdot s / V \cdot m$).

When the sensor is connected to a resistor R, the output voltage of the sensor is

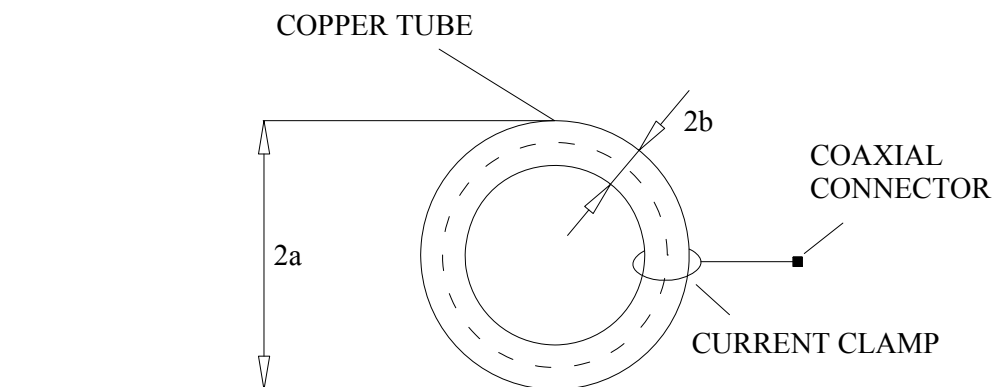$$V(t) = I(t) \cdot R = 3\pi r^2 R \varepsilon_0 \frac{dE(t)}{dt} \tag{31}$$

COPPER TUBE

2b

COAXIAL
CONNECTOR

2a

CURRENT CLAMP

Fig. 8. Closed circular loop (CCL) sensor.   2a = diameter; 2b = loop width.

conducting sphere

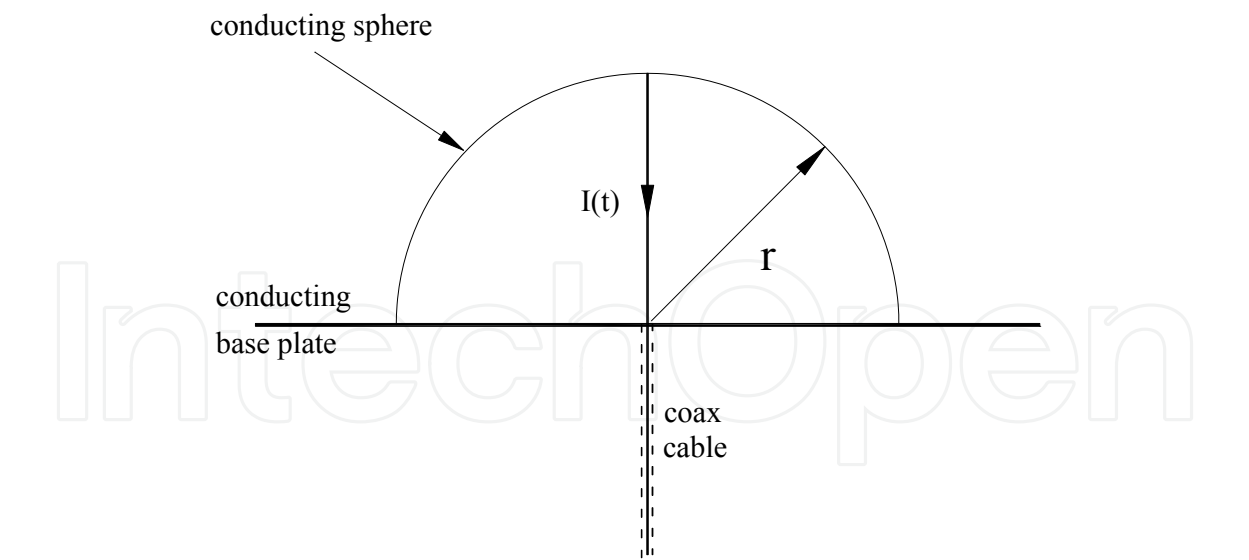I(t)

r

conducting
base plate

coax
cable

Fig. 9. Hollow spherical dipole (HSD) sensor

The output voltage is related to the time-derivative of the electric field. The sensor factor is found to be

$$F_e(t) = \frac{E(t)}{\int_{\tau_i} V(t)dt} = \frac{E(t)}{3\pi r^2 R\varepsilon_0 \frac{1}{\tau_i}\int_0^t \frac{dE(t')}{dt'}dt'} = \frac{\tau_i}{3\pi r^2 R\varepsilon_0} \quad [V/m/V] \tag{32}$$

The sensor factor depends on some constants, the sphere radius r, resistor value R and the integration time τ_i. Integration is necessary to relate the output voltage $V(t)$ to the electric field $E(t)$. This integration can be done by using a passive or active integrating circuit in the output signal line of the sensor. Also, a numerical integration is possible.

Electromagnetic (EM) Field Measurement
The task of EM fields measuring we can find in international EMC standard EN 61000-4-3,which describes measurement of electric devices immunity against RF fields (Dixon and Dutcher 1990). The electromagnetic environment is determined by the strength of the electromagnetic field, is not easily measured without sophisticated instrumentation nor is it easily calculated by classical equations and formulae because of the effect of surrounding structures or the proximity of other equipment that will distort and/or reflect electromagnetic waves. Tested equipment is subjected to field strength of 3 V/m or 10 V/m with homogeneity –0dB/+6dB from 80 MHz to 1000 MHz. This frequency range is 80% amplitude modulated with a 1 kHz sine wave. The signal generator provides the modulated frequency at a step rate of 1% of fundamental to the RF amplifier. The RF amplifier provides the necessary power to the antenna to establish the field levels as monitored by the field probe. The anechoic chamber, where the test is performed, is calibrated according to the criteria as per EN 61000-4-3 for 16 points given by geometrical arrangement in Figure 10 (2006, Bittera et al. 2006).
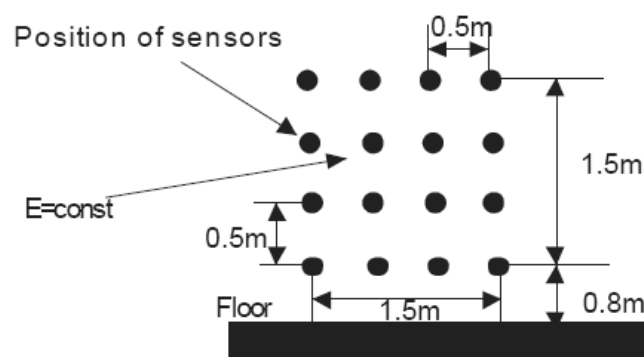

Fig. 10. Geometrical arrangement of measuring points

Then main task is setting the proper value of field strength at the place of tested device; or measuring of EM field. Because field strength is monitored by probe without tested device at test place result of measurement is influenced only by the presence of the probe, this process is not very easy and quality of evaluation depends just on the field probe.
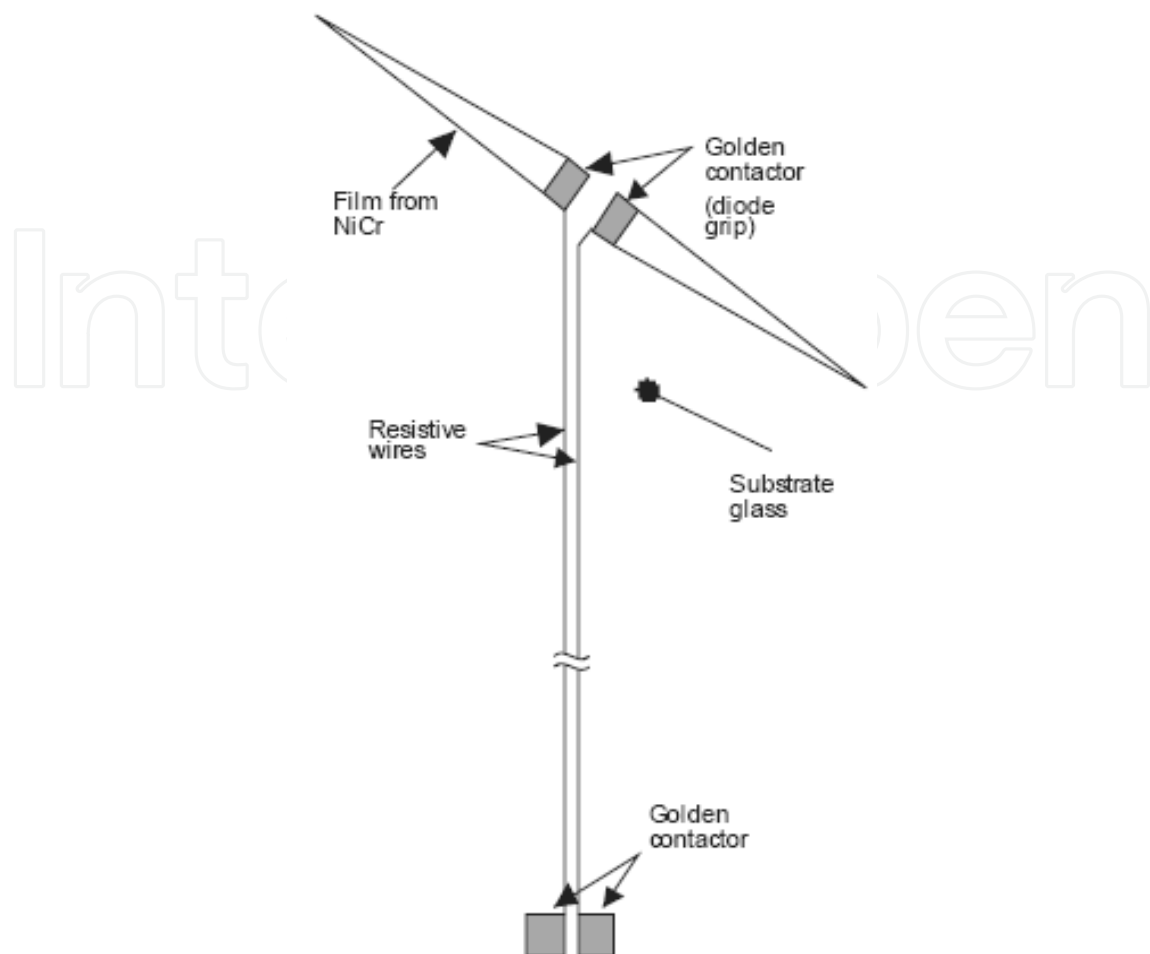*a. EM field probe*

Fig. 11. Measuring resistive dipole(Bittera et al. 2006)

The task of field probe is to transform the electrical field into directly measurable quantity as e.g. DC voltage is. The heart of probe is sensor, which is often realized as a dipole with travelling wave. This sensor works in an ultra-wide frequency range, it has a sufficient sensitivity and its producing is not very difficult. Voltage induced on a dipole is directly proportional to strength of incident EM field. This voltage is rectified and transferred via resistive wires to electronic interpretation unit (EIU) that is located in a sufficient distance from sensor. Scheme of sensor can be seen in Figure 11, to the golden contact we connect EIU, it converts signal into digital form and transfers it to the controlling computer. In fact, probe consists of three independent sensors due to isotropic properties of the whole probe. In term of measurement the field around sensors is interested for us. This field can be affected by metal parts of probe as enclosure of EIU or sensors are.

b. Model of the probe

It is necessary to know how can be the EM field influenced by presence of the probe during the measurement. To solve this problem, we have to design such a model, which can represent real behavior of the probe and is also designed regarding to the used method. In the case EM field is excited by point source and waves propagate to surroundings and the main task is to calculate the strength of EM field, or current distribution on attendant structures in analyzed area eventually. Such problem leads integral equation that can be described formally

$$\iiint_V \nabla X dx dy dz = Y \tag{33}$$

Where Y is source and X unknown function V analyzed area and ∇ is the Hamiltonian operator.

It means that using unknown function X can be solved, which in the case represents EM field distribution in V and Y is the feed of EM field source. Solution of the function leads to integral equation of first kind, which has not any analytical solution. Hence, we can transform it to integral equation of second kind or solve this equation numerically. However transformation to the integral equation of second kind is very difficult, complex and just approximate, so numerical solution, which is quite accurate, is preferred. One of the most popular methods is method of moments that is based on transformation of integral equation to system of linear equations – matrix equation and it can be solved easily using computer. This principle is used by much commercial software that solves EM problems, e.g. FEKO, NEC, etc.

Method of moment's principle is based on dividing analyzed structures to the small parts, called segments. If one has more segments it means that one needs more long time calculation, but has more accurate results. So it is necessary to strike a balance between number of segments and calculation accuracy. To get the model of probe all the metal parts (case of EIU and sensors) were replaced with segments with properties (dimensions, electrical properties) as real probe has (see Figure 12). We consider that probe is situated in infinitely large space without any caterers and it is incident by plane wave with linear polarization. The distance between sensors and case of EIU can be changed, in case of probe the distance is h = 30cm.
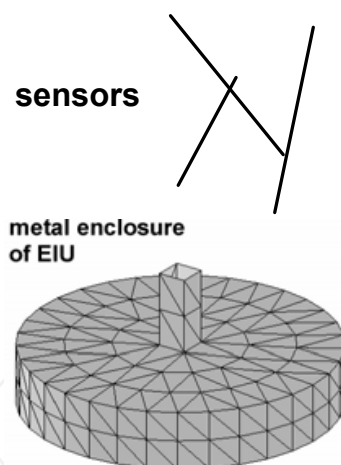

Fig. 12. Model of the probe in simulation(Bittera et al. 2006)

Spatial Electromagnetic Field Sensor

This is made up into a structure in which an electric-current sensor that detects the change in the spatial magnetic field due to the electric current passing through the overhead transmission/distribution line and that is comprised of a core and coil and a voltage sensor that detects by a plate electrode the line voltage capacitance-divided by the spatial charge between an electrically charged portion of the overhead transmission/distribution line and a plate electrode insulated from the earth, both, are accommodated in a hermetically sealed sensor container, such as Figure 13.
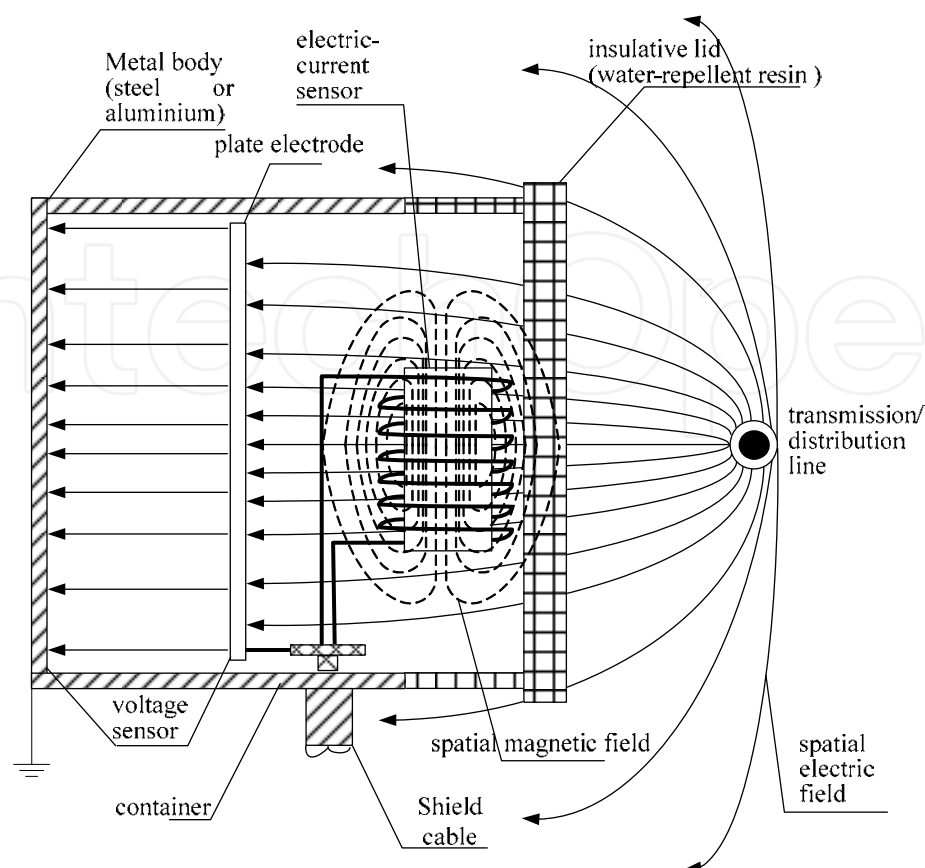
Fig. 13. Container of spatial electromagnetic field sensor

A noncontact sensor comprising a container including a container main body having an opening portion at one side and an isolative lid member that hermetically seals said opening portion of said container main body, and a voltage sensor disposed in said container in the way in which a lid member side is opposed to an electrically charged portion of an overhead wire line, being insulated from the earth, detecting a voltage that is induced in a plate electrode due to a spatial charge between said electrically charged portion and the plate electrode within said container, characterized in that said lid member has a structure in which a water-repellent layer constructed using a water-repellent resin is provided on the whole or a part of its at least exposed surface (Nakamura 2008).

The above-described "container main body" is a container in which a plate electrode and the like are accommodated and shielded so that they are not affected by a surplus magnetic field and a surplus electric field. The container main body like this can be made of metal such as stainless steel and aluminum. Also, the container may be a resin-made container on which an electrically coating material and the like are coated so as to add an effect of shielding an electric field, etc.

2.3.3 Sensors for faults generated temperature changing

Distributed fiber-optic temperature sensors (DTS) were first proposed in the early 1980s and have been commercially available since 1987. They are instruments which use an optical fiber, both as a temperature sensor and as a means of bringing the information back from the sensor to the terminal equipment.

Because distributed temperature sensors use optical fibers as the sensing and communications element, they can be used in electrically noisy environments without any problems of interference. The fact that a single fiber is able to replace many thousands of thermocouples simplifies wiring considerably and thus allows the technology to be used in applications where space, weight or wiring costs preclude traditional point sensors. An additional benefit of the technology is that the sensors can be made entirely from dielectric materials and in that sense are intrinsically safe(Hartog 1995).

The operation of distributed temperature sensors is based on the optical time domain reflectometry (OTDR) technique, in which a short pulse of light is launched into the fiber and the return signal is analyzed. The time from the launching of the pulse can be mapped directly into distance along the fiber---in a similar way to the measurement of target range in radars. The signal consists of light scattered by the glass in which the interrogating pulse is traveling. Some of the wavelength components (in particular the so-called Raman anti-Stokes band) in the return signal are temperature-sensitive and these are used to determine the temperature along the fiber. In order to separate the temperature variations from other factors which also influence the Raman backscatter signal, several referencing methods are used, including comparison with other wavelengths which are less sensitive to temperature and repeating the measurement, but launching into the opposite end of the fiber (the latter then being installed in a loop configuration). In this way, an accuracy of +0.3℃ can be achieved.

The most advanced application for distributed temperature sensing in the power supply industry is in the monitoring of high voltage power cables. The capacity of a power transmission cable is limited by the increase in core conductor temperature caused by resistive heating as the current is increased. The maximum operating temperature is limited by degradation mechanisms in the insulation materials used. Traditionally, cables have been rated from detailed models which take into account the design of the cable, but also the ability of the soil surrounding the cable to dissipate the heat. Thus a cable running through a dry soil is less able to dissipate its self-generated heat than one laid in wet conditions.

The soil conditions are not necessarily known at all points along the cable at all times. Moreover, other factors affect the temperature along the cable, such as the proximity of other cables or services (e.g. district heating). The presence of these services may not always be known at the time when the cable is planned. Of course, it is the temperature of the hottest point along the cable which limits its capacity and the location of the hottest point is not always known. Energy cables are therefore usually operated below their maximum capacity, even at times of peak demand.

A cable with an optical fiber distributed sensor, either integrated within the cable, or laid in physical contact with the sheath can significantly reduce the uncertainty in determining the core temperature along the cable. This allows the cable to be operated with confidence at loads much closer to the maximum design value. The practical benefits are that knowledge of the temperature profile helps the utilities to meet peaks in demand with a smaller number of cables. Ultimately, the approach may allow cable sizes to be selected less conservatively, with cost savings well in excess of the cost of the monitoring equipment.

The temperature profile of cables can be measured by temperature sensor. The temperature distribution is extremely non-uniform; the peaks in temperature in this case are believed to be caused by the cable crossing other underground services. Once their location is known, only a few hot spots need be monitored by the operator, although it is possible for the

relative magnitude of the hot spots to vary according to seasonal variations in the load of the cable and of neighboring services, and the distributed nature of the monitoring thus remains of value throughout the life of the cable.

3. Fault detection methods

3.1 Fault detection methods with fundamental frequency signals

3.1.1 Faults detection with harmonic current comparison

A typical ineffectively earthed distribution system is shown in Figure 14. And its zero sequence equivalent circuit with single-phase grounding fault is shown as Figure 15. The capacitance to earth of the Feeder 1 is C_1, and that of the Feeder n is C_n. The Feeder j is the faulted feeder. Peterson-coil inductance is L_n and zero sequence voltage of the faulted point is $\dot{U}_{0f}$ (Zeng et al. 2007).
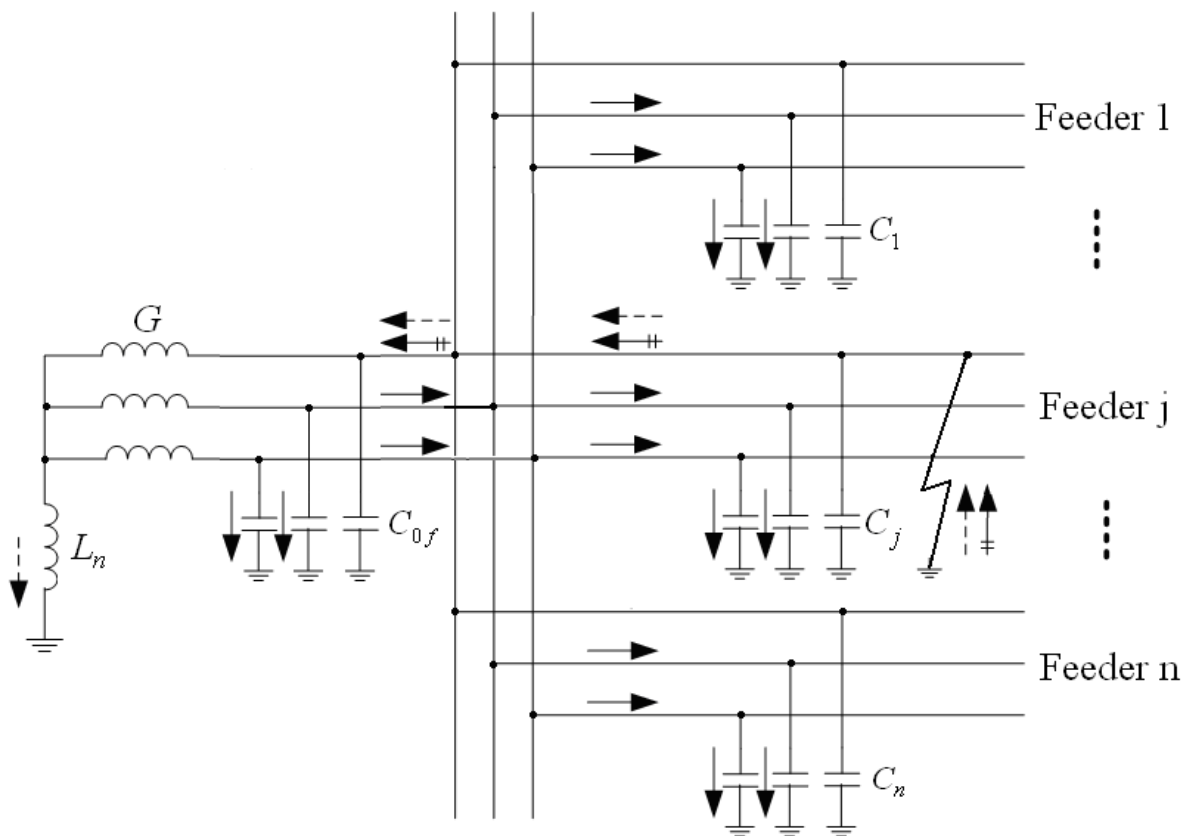
Fig. 14. Ineffectively earthed distribution system with single-phase grounding fault
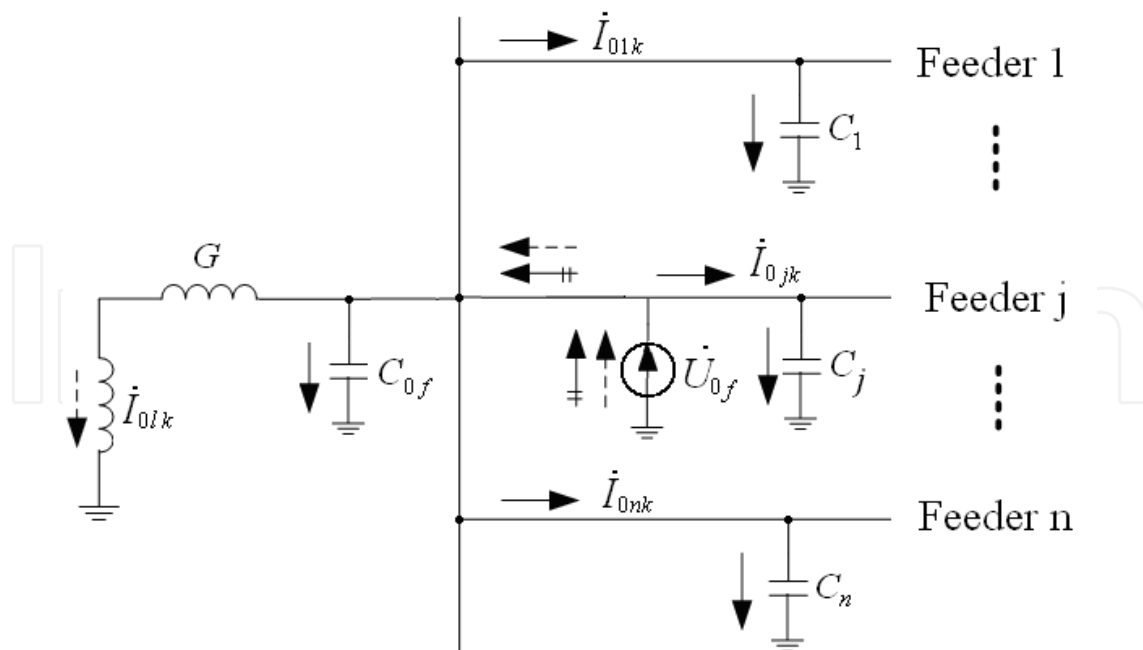
Fig. 15. Zero sequence equivalent circuit of ineffectively earthed distribution system with single-phase grounding fault

Grounding faults generate transient signals. They include many different frequency harmonic components. The components are produced in the faulted point, flow to the source and normal feeders. From Figure 15,

$$\dot{I}_{0lk} + \dot{I}_{ojk} + \sum_{i=1, i \neq j}^{n} \dot{I}_{oik} = 0 \tag{34}$$

Namely
$$\dot{I}_{ojk} = -(\dot{I}_{0lk} + \sum_{i=1, i \neq j}^{n} \dot{I}_{oik}) \tag{35}$$

Where, $\dot{I}_{olk}$ is the kth harmonic current of the zero sequence component in the Peterson-coil, $\dot{I}_{oik}$ is the kth harmonic current of the zero sequence component in the Feeder i, $\dot{I}_{ojk}$ is the kth harmonic current of the zero sequence component in the faulted feeder (i =1,2,...,n; j=1,2,...,n).

The inductive reactance will increase and the capacitive reactance will decrease along with the increasing of the harmonic order. Considering the zero sequence current, when the power system capacitive current flowing in the normal feeder is much larger than the inductive current flowing in the Petersen-coil, as $\sum_{i, i \neq j}^{n} \dot{I}_{0iM} >> \dot{I}_{0lM}$, the Mth harmonic inductive current compensated by the Peterson-coil can thus be ignored. Namely the current of the Mth harmonic component in the faulted feeder is almost the sum of the current in sound feeders, and the Mth harmonic component direction in the faulted feeder is just opposite to that in the sound feeders. The faulted feeder can thus be detected by utilizing

the Mth harmonic component. The feeder with Mth harmonic current component larger than other feeders and direction opposite to other feeders is the faulted feeder.

The M is often selected as 5, and the fifth harmonic component is often used to detect the grounding feeder in China. In practice, power transformer also generators 5th harmonic. It sometimes disturbs the 5th harmonic generated by grounding faults and has influenced on the fault detection. Moreover, the 5th harmonic current is relation to fault arc and resistance. Different type faults have different 5th harmonic, and have different fault detection characteristics. So the 5th harmonic current based grounding fault detection has some limits.

3.1.2 Faults detection with signal injection

A signal current is injected to the grounding fault phase of faulted feeder through bus voltage transformer. The signal frequency is between n and $n+1$ times the power fundamental frequency 50Hz:

$$n \cdot 50 < f_0 < (n+1) \cdot 50 \tag{36}$$

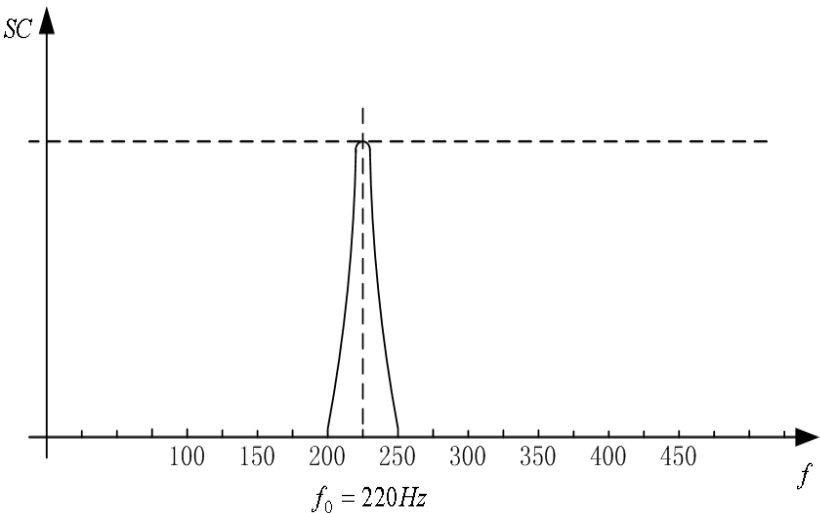The signal frequency is set as 225Hz shown as Figure 16 (Zeng et al. 2007).

Fig. 16. Frequency character for current

A special designed detector is installed in every feeder to detect the injected signal. In normal conditions, the signal magnitude in every feeder is in direct proportion to its capacitance to earth. In grounding fault conditions, the signal is flowing to the fault point from the signal source, and the signal magnitude in every normal feeder is almost zero. The faulted feeder can thus be detected by measuring injected signal magnitude.
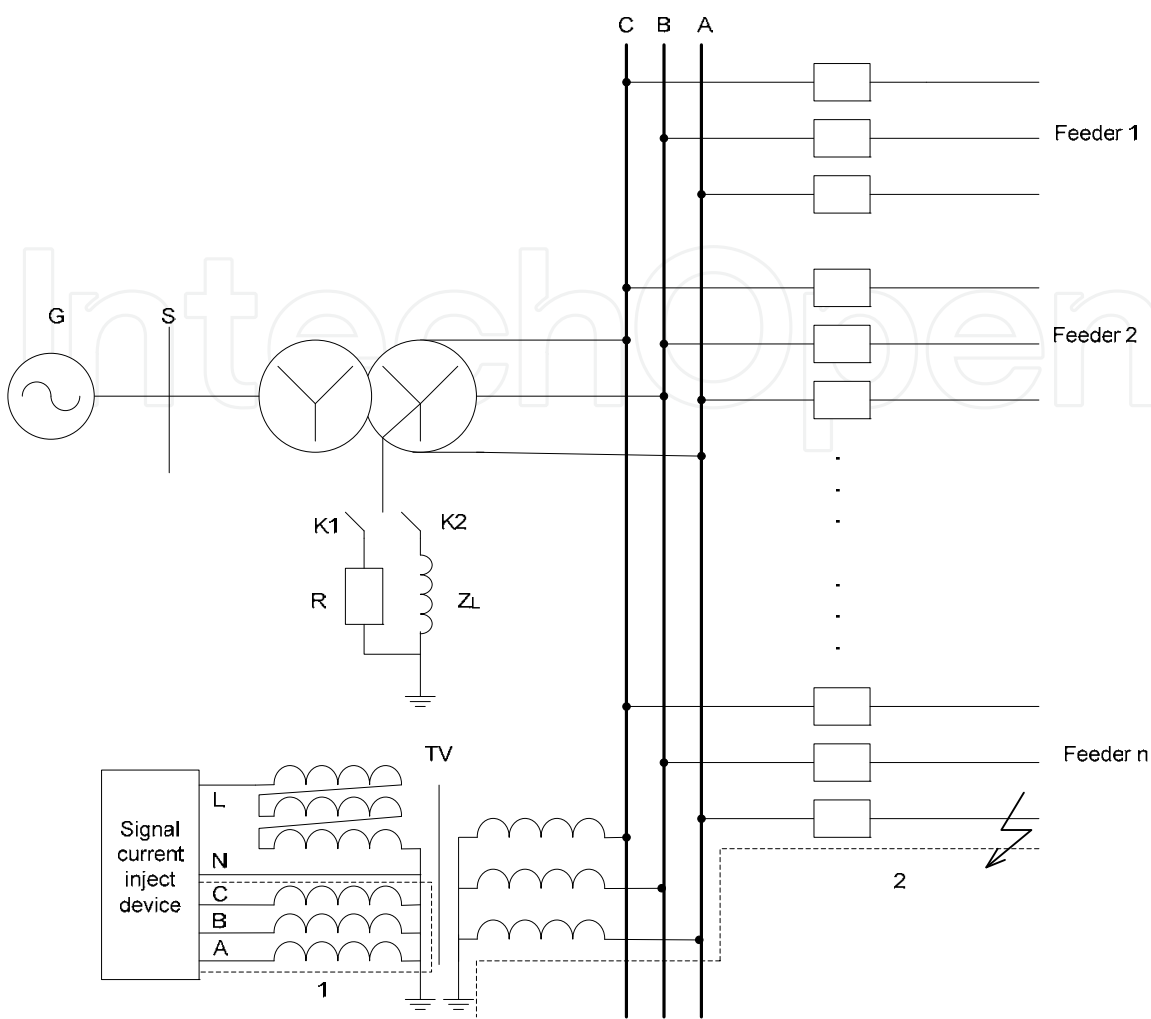
Fig. 17. Signal injection circuit

The fault detection scheme can be described as below. When the distribution system is in normal condition, no tested signal is injected to the system, and the signal detector tested signal magnitude is zero. When grounding fault occurs, the fault phase voltage A will decrease to zero, for example phase A fault, whereas the voltage of the normal phase B and phase C will rise up to the line voltage, namely $\sqrt{3}$ times the phase voltage. The signal injector device then inject signal from the phase A secondary of transformer to the power system. And the signal current flows to the fault point (shown as Figure 17 and 18); the signal in every normal feeder is almost zero. The faulted branch can also be detected by tracking the injection signal.
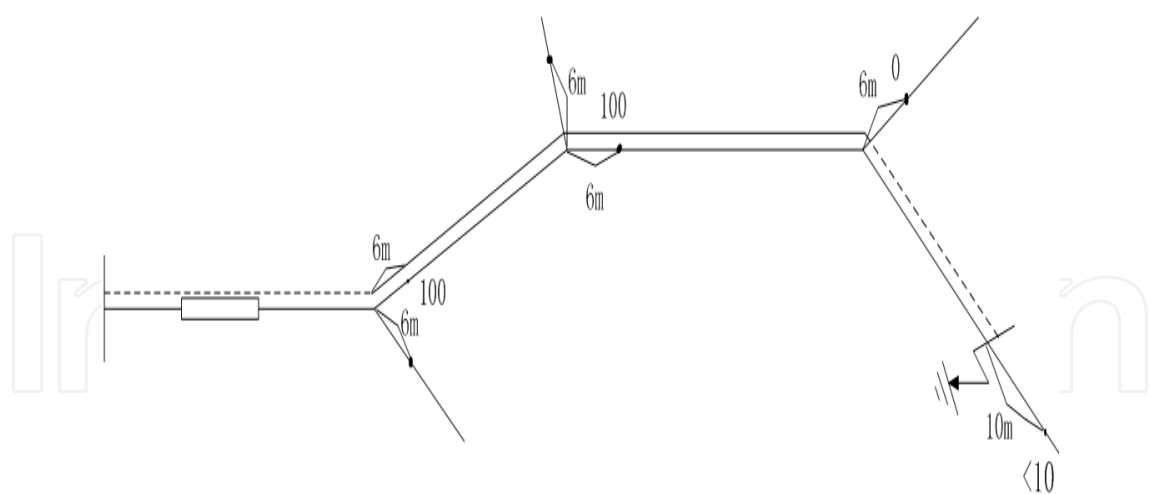
Fig. 18. Injection signal flowing from source to fault point

Feeder No.	Grounding Fault Times	Correct Fault Detection Times	Time Saving for Fault Isolation (h)
1	4	4	2
2	3	3	1.5
3	5	5	2.5
4	6	6	3
5	7	7	2
6	9	9	2
7	1	1	2
8	3	3	1.3
10	2	2	2
11	7	7	2
12	5	5	2
13	1	1	1.25

Table 1. Fault detection results for Sanjiang Substation

The signal injection based fault detection method has been applied in more than 2000 distribution systems. An operation statistic results in the Sanjiang Substation (Zengchen Power Company) is shown as Table 1. All faulted feeder can be detected correctly, and faults isolation time can be saved. The signal injection based detection method has some advantages:

a. The injected signal is small, and it only flows into the grounding fault point. It has no influence for power system normal operation.

b. The special signal current detector is installed near each feeder to detect the injected signal, it is easy to install.

c. When grounding faults occurs, the faulted point can also be determined if the operator holds the special signal current detector moveing along the faulted feeder to find the point which the injected signal current disappears.

Whereas, arcing faults is difficult to detect by the method because of the harmonics interference caused by earth faults. And high impedance grounding fault is also difficult to detect, because the signal is too small to detect in the faulted feeder.

3.1.3 Faults detection with phase current difference

In three-phase-symmetry systems, grounding faults caused changing currents have been analyzed in section 2.1. The difference between three phase changing currents in sound feeder is nearly zero. The difference between the healthy and fault phase changing currents in fault feeder is very large, equaling to the residual current. And the difference between healthy phase changing currents in the fault feeder is also relatively small, almost equaling to zero. If the difference is larger than a threshold, grounding fault can be detected in the tested feeder.

The technique of sampled value difference protection has been widely applied in compute based protections due to its inherent simplicity and good performance, which uses instantaneous sampled values to calculate the difference of currents, and checks whether samples satisfy the operating criterion or not. The number of satisfied samples in a system frequency cycle is larger than a threshold, fault can be detected (Wang et al. 2007, Wang et al. 2006).

The difference protection is implemented with different phase sampling values comparing. The operation criterion is:

$$i_d(k) \geq K_1 i_r(k) + i_{d0} \tag{37}$$

Where K_1 is restraint coefficient, k is sampling number, i_{d0} is pickup current, $i_r(k)$ is instantaneous current, and $i_d(k)$ is instantaneous difference current which can be calculated by:

$$i_d(k) = \max\left(\left|\Delta i_A(k) - \Delta i_B(k)\right|, \left|\Delta i_B(k) - \Delta i_C(k)\right|, \left|\Delta i_C(k) - \Delta i_A(k)\right|\right) \tag{38}$$

Under normal conditions, the difference between healthy phase changing currents would be equal to zero. Considering the influence of measuring error, it would be a small value. In order to limit the influence, i_{d0} can be obtained by:

$$i_{d0} = \left|\Delta i_B(k) - \Delta i_C(k)\right| \tag{39}$$

In order to improve the protection precision, the sampling rate of the protection is set as 32 samples per cycle. Taking the half cycle for example, set R=16. During a period after the fault, instantaneous difference current ($i_d(k)$) is calculated by (38). When $i_d(k)$ is satisfied operation criterion (37), grounding fault can be detected in the protected feeder. Namely, if there are S samples satisfying (37) during the continuous R sample's judgments in half system frequency cycle after fault inception, the protection would operate. As long as the number of the (37) satisfied sampling number is less than S, the protection would not mal-operate.

Fig. 19. Prototype of FTU
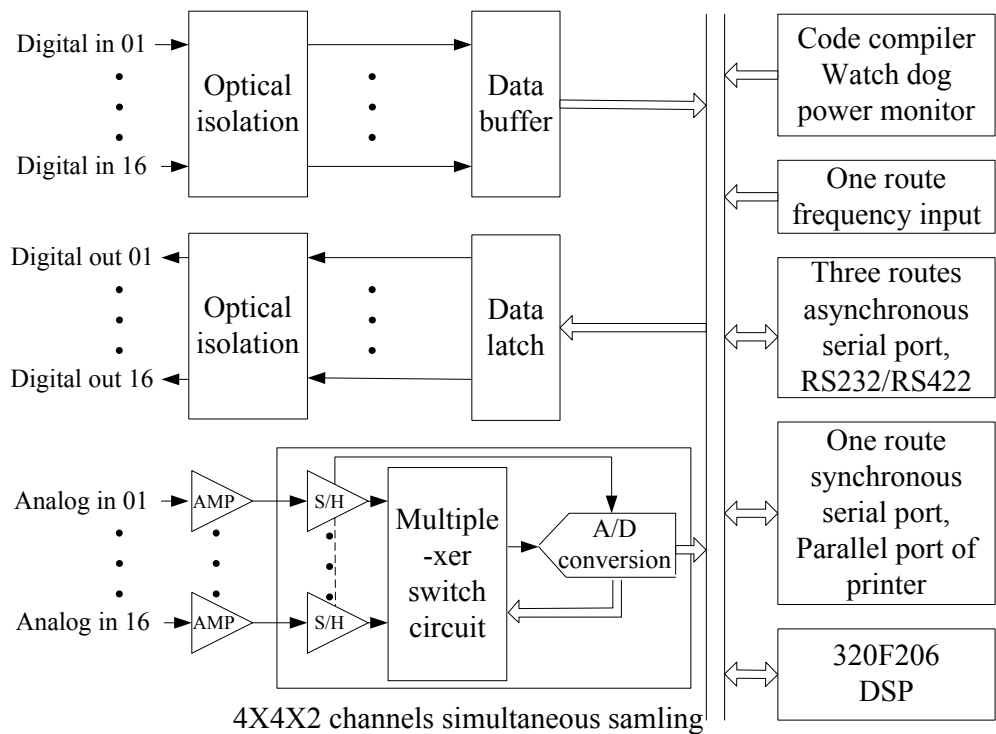

4X4X2 channels simultaneous samling

Fig. 20. Principle of FTU hardware frame

The protection scheme only utilizes the measured voltages and currents in the protected unit, and does not need the parameters of the distribution system or other unit. It can be implemented on feeder terminal units (FTU) with three-phase voltages and three-phase currents sampling in the distribution automation systems. The FTU prototype (shown as in Figure 19) has been developed. It uses with DSP TMS320F206, and its hardware frame is showed as Figure 20 (Zeng et al. 2008).

The phase current difference based detection method has been tested in laboratory. High impedance faults and arcing faults can be detected with high precision. Not enough phase current difference based fault detectors have applied in power system.

3.2 Fault detection methods with transient signals

When a fault occurs on a transmission line, the voltage at the point of fault suddenly

reduces to a low value. This sudden change causes a high frequency transient that propagates away from the fault point in both directions along the line at a velocity almost equal to the speed of light. The high frequency transient is called traveling waves which can be used for fault point detection. When the initial traveling wave reaches an impedance discontinuity, such as a substation, a part of the wave is reflected back along the line towards the fault. The remainder is transmitted through the substation into the network. These traveling waves continue to be divided into reflected and transmitted waves and their amplitude attenuates with time until finally a new equilibrium is reached.
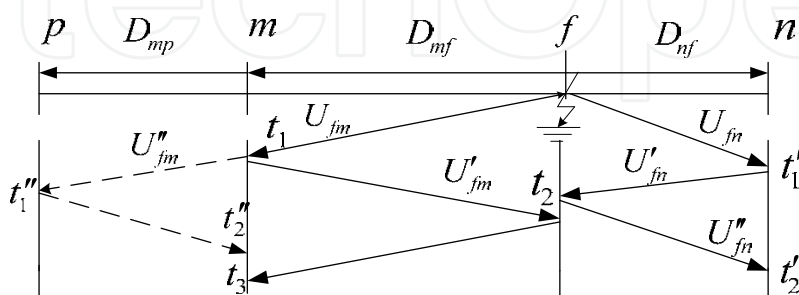

Fig. 21. Transport network of traveling wave in transmission line

Supposing that the fault occurs at f, the transport network is shown in Figure 21 (Zeng. 2000). The initial traveling wave propagates away from the fault in both directions along the line, and produces refraction and reflection at point of m, n and p. U_{fm}, U_{fn} are the initial traveling wave from fault point f; U'_{fm}, U'_{fn} are reflection traveling wave at point m, n; U''_{fm} is refraction traveling wave at point m (the refraction traveling waves from point p and n are not signed in Figure 21).

Taking point m as an example, reflection coefficient α_m and refraction coefficient β_m can be expressed as follows:

$$\alpha_m = \frac{Z_1 - Z_m}{Z_1 + Z_m} \tag{40}$$

$$\beta_m = \frac{2Z_1}{Z_1 + Z_m} \tag{41}$$

Where, Z_1 is equivalent wave impedance of non-fault line which is directed connected with bus m, Z_m is equivalent wave impedance of fault line, generally valued for 300Ω.

3.3 Fault detection methods based on information fusion or AI technology

Different fault detection methods usually operate using different fault information. They have different applications with different degrees of precision and robustness. In practical operation, a single ground fault protection scheme has poor precision in ground fault detection. If all kinds of fault information can be integrated and fused, the effect of the disturbing signal can be reduced, inherent limitation of the single protection scheme can be eliminated and the precision and robustness of fault detection can be improved .

Information fusion or AI technology is an intelligent information processing method, and it is

the process of combining data to refine state estimates and predications. The purpose of information fusion is to produce information from different sources in order to support the decision-making process (Bossé et al. 2006).

3.3.1 Fault detection methods based on Neural Networks

Neural networks (NN), which are parallel distributed information processing units with different connection structures and processing mechanism, are particularly suitable to link the different variables of a power system where the relationship between the independent and the dependent variables are not easily quantifiable. Neural networks are robust to input and system noises, have learning capabilities, and can perform in real time (Lippmann 1987). Indeed, neural networks can be viewed as nonlinear adaptive system identification units, which rely on pattern recognition for the identification procedure (Widrow and Winter 1988).

The NN structures used in the fault detection are of the multilayer perceptron type, trained using the backpropagation algorithm. The basic philosophy of neural networks learning procedure is presented in Figure 22, where the weights are updated based on the error generated through the comparison of neural output and the target output. The typical single layer net is shown in Figure 23. The input vectors are selected variables derived from the transducer signals.
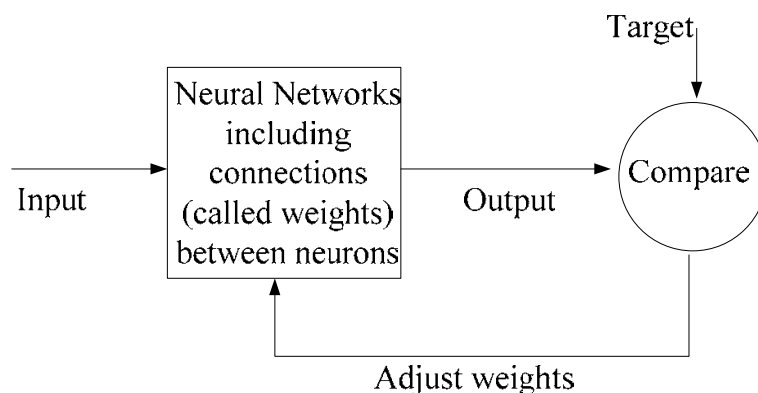

Fig. 22. Neural Networks philosophy(Awais 2003)

Training a network by backpropagation involves three stages:
a. The feedforward of the input training pattern
b. The back propagation of the associated error
c. The adjustment of the weights

During the learning process, the NN weights are adapted in order to create the desired output vectors. For learning process, the symptom-fault map is required. There is also the possibility of a hybrid learning process, simulated data for healthy and faulty machines. In this way, the NN can learn the health condition (Awais 2003).

The time domain signals both in healthy and faulty machines are passed through the low pass filter. Then the time domain signal is changed to frequency domain by fast Fourier transform (FFT). The magnitude from FFT is used as input vector for training the NN which defines the target as healthy or faulty. After training NN, we have the weight and bias for using to detect the faulty machine.
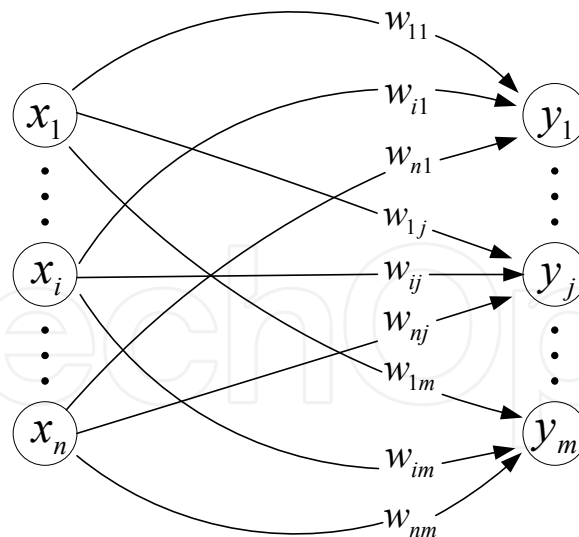
Fig. 23. A single-layer neural net

The dynamics of the system with out faults is represented by (Sreedhar et al. 1995):

$$\dot{x} = Ax + Bu + \Psi(x,u) \tag{42}$$

The dynamics of the system due to the occurrence of the fault is represented by

$$\dot{x} = Ax + Bu + \Psi(x,u) + \Phi(x,u) \tag{43}$$

Considering a sigmoid neural network whose input–output characteristics are described by:

$$y = \hat{\psi}(q,\dot{q},\tau;\hat{\theta}) \tag{44}$$

Where $(q,\dot{q},\tau) \in \mathfrak{R}^n \times \mathfrak{R}^n \times \mathfrak{R}^n$ is the input to the network, $y \in \mathfrak{R}^n$ is the output of the network and $\hat{\theta} \in \mathfrak{R}^p$ represents the adjustable weights of the network. Let the weights $\hat{\theta}(0) \in \hat{\theta}_0$ of the selected neural network be initialized such that

$$\hat{\psi}(q,\dot{q},\tau;\hat{\theta}_0) = 0, \quad \forall q,\dot{q},\tau \tag{45}$$

corresponding to the no-failure situation. Note that this can be achieved simply by initializing the output weights of the network to zero(Vemuri et al. 1998).

Artificial neural networks have been widely used partly because of their multi-input parallel processing capabilities, which are most suitable for real time applications. A large number of input variables can be simultaneously fed to a multi-input neural network. Despite the increase in the number of input nodes, the computation time of the network remains the same because neural nets perform parallel processing. Thus, increasing the number of input nodes does not affect the neural network processing speed. Besides, increasing the number of inputs nodes increases the robustness of the neural networks with respect to measurement noise. Moreover, once designed, the internal structure of artificial neural networks can be easily changed, if modifications or additions need to be made. The network can be updated, without much difficulty, by merely retraining it a few times more after the network structure is modified (Chow and Yee 1991).

3.3.2 Fault detection methods based on Fuzzy Algorithm
The output result of the single ground fault protective relay is either fault or no fault. If 1 is

applied to represent fault, and 0 is applied to represent no fault, the output value of the ground fault protection can be chosen from the data collection {0, 1}. The principle of fuzzy ground fault protection is described as following. The subjection degree of element to data collection is extended to choose any value from data section [0, 1], comparing to choosing from data collection {0, 1} formerly. Output uncertainty of different ground fault protective relays can be expressed by the subjection function. And the faulted feeder can be identified by clarifying the fuzzy results.

The subjection degree function μ_i of an arbitrary ground fault protective relay i can be selected according to practical instance, such as normal function, trigonometric function, trapezoid function, S function and break-line function etc. As shown in Figure 24, the break-line subjection degree function is selected, where S is the tripping threshold of the general ground fault protective relay, S_L is the possible lower limit of tripping threshold in the case of fault, S_H is the possible upper limit of tripping threshold in the case of non-fault. Because the result of a single fault protection scheme isn't reliable in the section [S_L, S_H], this section is defined as fuzzy section. The possibility of fault in this section can be described by fuzzy subjection degree.
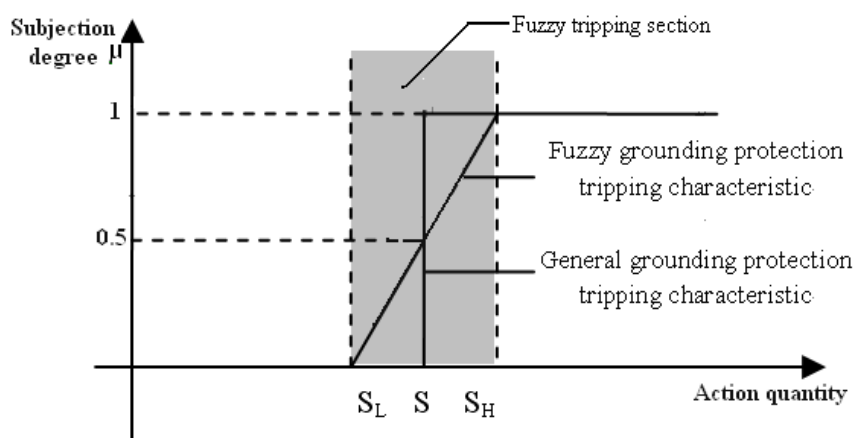

Fig. 24. Subjection degree function of a grounding protection action(Zeng et al.2004)

There are many methods for calculating fuzzy information fusion, which usually adopt additional calculations considering the characteristics of ground faults. The gross reliability of fault decision-making can be expressed as the sum of products of different subjection degree and fuzzy reliability coefficients. For example, the fuzzy reliability coefficient of the ground fault protective relay i is K_i according to expert experience. It's value domain is from zero to one. By addition calculation, the information fusion output of total ground fault protective relays is

$$Y = \sum_{i=1}^{n} K_i \mu_i \tag{46}$$

The clarifying process of fuzzy reliability degree is converting fuzzy reliablity degree into practical output judgement (fault or no fault) according to fuzzy principle. For example, when $Y \geq 0.5$, there is fault happening in this distribution line; when $Y < 0.5$, there is no fault happening in this distribution line.

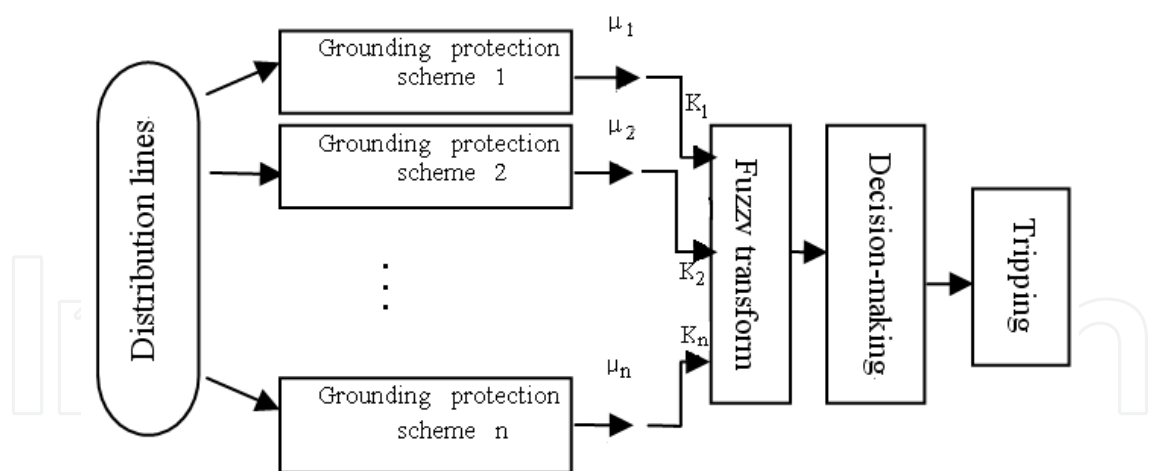The scheme for information fusion is shown as Figure 25.

Fig. 25. Schemes of fuzzy grounding fault detecting(Zeng et al.2004)

3.3.3 Fault detection methods based on Genetic Algorithm

Genetic algorithms (GA) are probabilistic search techniques inspired by the "survival of the fittest" principle of the neo-Darwinian theory of natural evolution, and by the mechanisms of natural genetics. This algorithm looks for the fittest individual from a set of candidate solutions called population. Basic operations are selection, reproduction, crossover and mutation. Parent selection gives a higher probability of reproduction to the fittest individuals. During crossover some reproduced individuals cross and exchange their genetic characteristics. Mutations may occur in a small percentage and cause a random variation in the genetic material, thus contributing to introduce variety in the population. Fitness function of each individual is changed by crossover and mutation operators. The selection operator decides whether an individual survives in next generation or not. Roulette wheel and tournament selection are two common selection methods. The steps of genetic algorithm are depicted in Figure 26 (Amaral et al. 2007, Aydin et al. 2008).
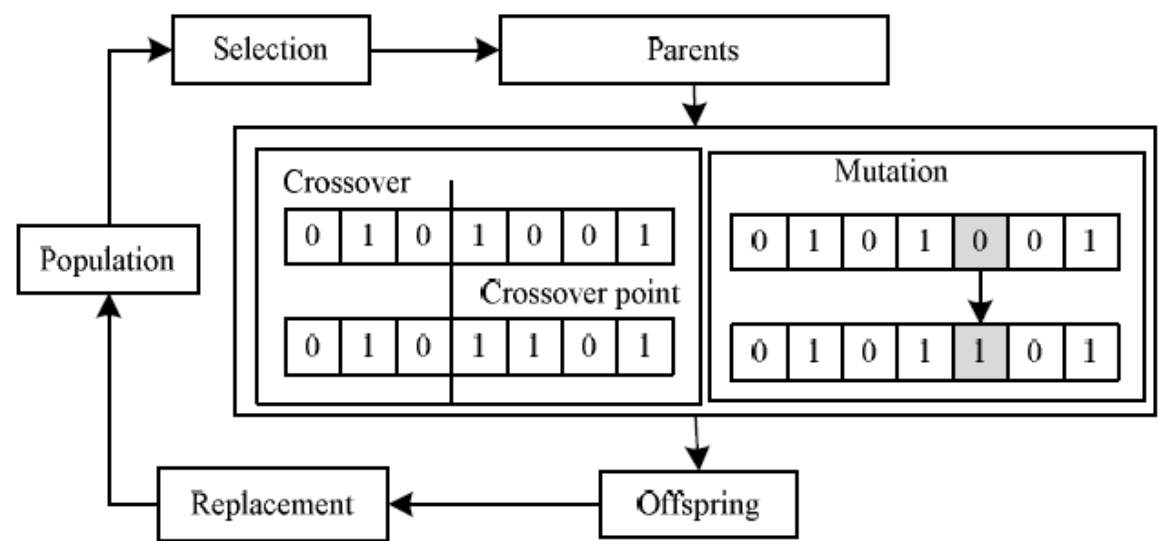
Fig. 26. Steps of Genetic algorithm

In every generation, a new set of artificial creatures $P(t)$ is randomly generated using bits

and pieces of the fittest members of the previous generation P(t-1). The process is repeated until the last generation P(t) does not satisfy the application requirements. A simplified sketch of the algorithm is shown in Figure 27 (Betta et al. 1996, Betta et al. 1998).

```
Procedure GA
    begin
    t:=0,
    initialize P(t);
    evaluate structures in P(t);
    while termination condition not satified do
        t:=t+1;
        select P(t) from P(t-1);
        recombine structures in P(t) using mutation and
        crossover;
        evaluate structures in P(t)
    end
    end.
```

Fig. 27. Sketch of the Simple Genetic Algorithm

For the robust ℓ_1 optimization problem the chromosome is constructed by formulating matrices A_e, W, P, H and N into a single vector Θ such that

$$\Theta = [V_{ec}(A_e)^T V_{ec}(W)^T V_{ec}(P)^T V_{ec}(H)^T V_{ec}(N)^T] \qquad (47)$$

The search region is then defined by establishing upper and lower limits $\underline{\Theta}$ and $\overline{\Theta}$ such that

$$\underline{\theta}_{ij} \leq \theta_{ij} \leq \overline{\theta}_{ij} \qquad (48)$$

If the stability criterion is not satisfied, a penalty is added to the cost such that

$$if \begin{cases} \max[\lambda_i(A_a)] < 1, & J = J \\ otherwise, & J = J + penalty \end{cases} \qquad (49)$$

where λ_i, $i \in (1, 2, \ldots, m + 2n)$ are the eigenvalues of the augmented system Aa (Curry et al. 2001, Curry and Collins Jr 2005).

4. Application of fault detection methods

4.1 Fault detection application in power system online monitoring

Many mining power systems utilize ineffectively grounded sources to restrict the residual current of single-phase earth fault in order to reduce outage and shock hazard. In practice, with the system expansion, topology changing and insulation aging, the potential residual current and zero sequence voltage for earth fault vary dynamically and some arcing earth

faults can easily cause over-voltage and induce multiple faults. In order to improve the system safety, on-site condition monitoring, safety evaluation for earth fault are proposed in this section.

System states can be classified into normal secure state, alert state, incipient fault state and fault state. In alert state and incipient fault state, some preventive actions need to be carried out. But in fault state, the faulty feeder section needs to be isolated.

Normal secure state

No fault exists in industry power system. Even if earth fault occurs, no high overvoltage and no large residual current will be caused, and arcing fault will be self extinguished.

Alert state

No fault exists in industry power system. But the neutral point-earth-impedance does not match to the system capacitance to earth. If earth fault occurs, the residual current or zero sequence voltage will be very high, so that some arcing fault will easily induce multiple faults. In order to improve it, neutral-point-earth-impedance adjustment (e.g. Petersen-coil tuning) is required.

Incipient fault state

Some very high impedance earth fault exists because of insulation aging, and so on. Although it does not cause overvoltage and affect system normal operation directly, it can create personnel and equipment safety problems, and has an adverse environmental impact. So some preventive actions need to be carried out.

Fault state

Earth fault occurs. It causes overvoltage and affects system normal operation directly. The faulty feeder section is required to be isolated as soon as possible.

Based on the above indexes, insulation intensity (dissipation factor), potential over-voltage and potential fault residual current, and the safety for earth fault in ineffectively earthed systems can be evaluated. When the safety indexes are over their threshold, an alarm will be given to the operator to change the system operation methods or carryout preventive maintenance. As shown in Figure 28, many parameters are measured online in normal mining power systems. When zero sequence voltage (U_0) is larger than its high threshold (U_{0set1}) which is often set as $30\% U_{ph}$, earth fault occurs. The fault feeder section can be detected by over-current protection with the injection current.

If a feeder's signal current (e.g. feeder k) is bigger than its threshold (I_{skset}),

$$I_{sk} > I_{skset} \tag{50}$$

this feeder is detected as the earth fault feeder.

The fault can be isolated automatically with distribution automation equipment. It works as one of remedial actions.
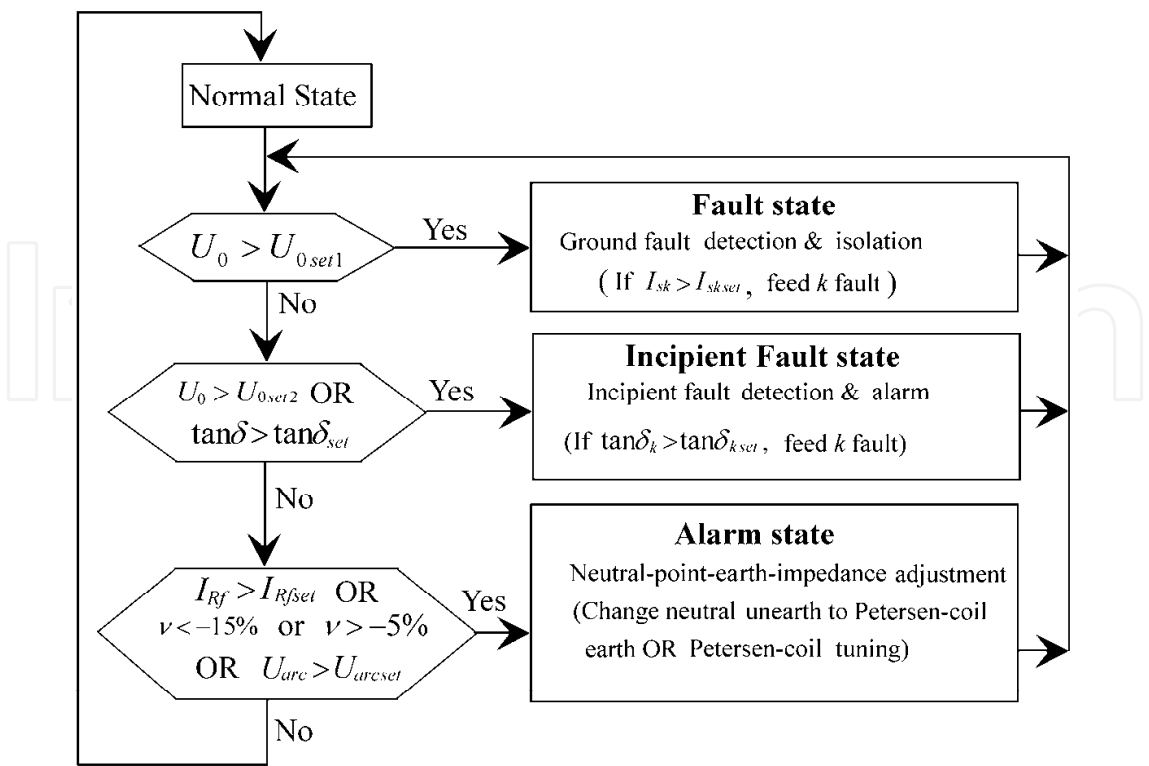
Fig. 28. On-site safety evaluation and security enhancement scheme (Zeng et al.2003)

If no fault existing, incipient fault will be tested. When zero sequence voltage (U_0) is larger than its low threshold (U_{0set2}) which is often set as 10% U_{ph}, or the total dissipation factor is larger than its threshold ($\tan\delta_{set}$) which is often set as 8%, incipient fault is detected. The feeder, whose dissipation factor is bigger than its threshold, is the high impedance earth fault feeder. An alarm is sent to the operator to maintain this incipient fault feeder.

If no fault and incipient fault existing, potential hazards will be evaluated. Supposed that some kind of earth fault occurs, it is assessed whether or not the potential residual current and overvoltage are out of their limits. In addition, resonance deviation in resonance earthed system is measured on-line. If some potential hazards for earth fault exist or resonance deviation is out of its limit, an alarm will be given to the operator to adjust neutral-point-earth-impedance. Some preventive action is usually carried out, such as: changing neutral unearthed or high resistance earthed to Petersen-coil earthed, Petersen-coil tuning, etc (Srivani and Vittal 2008).

4.2 Fault detection application in Power system condition-based maintenance

Condition-based maintenance (CBM) aims to detect latent failures on a basis of processing huge amount of information and then take actions to remove them (Liu et al. 2006). The main idea of CBM is to monitor the health of critical machine components and system almost continuously during operation and maintenance actions based on the assessed condition. If done correctly, CBM has the benefits such as reducing catastrophic failures, minimizing maintenance and logistical cost, maximizing system security and availability and improving reliability.

A CBM system usually has four major functional modules, namely feature extraction, diagnostics, prognostics and decision support. Figure 29 illustrates the relationship between these modules (Zhang et al. 2007).
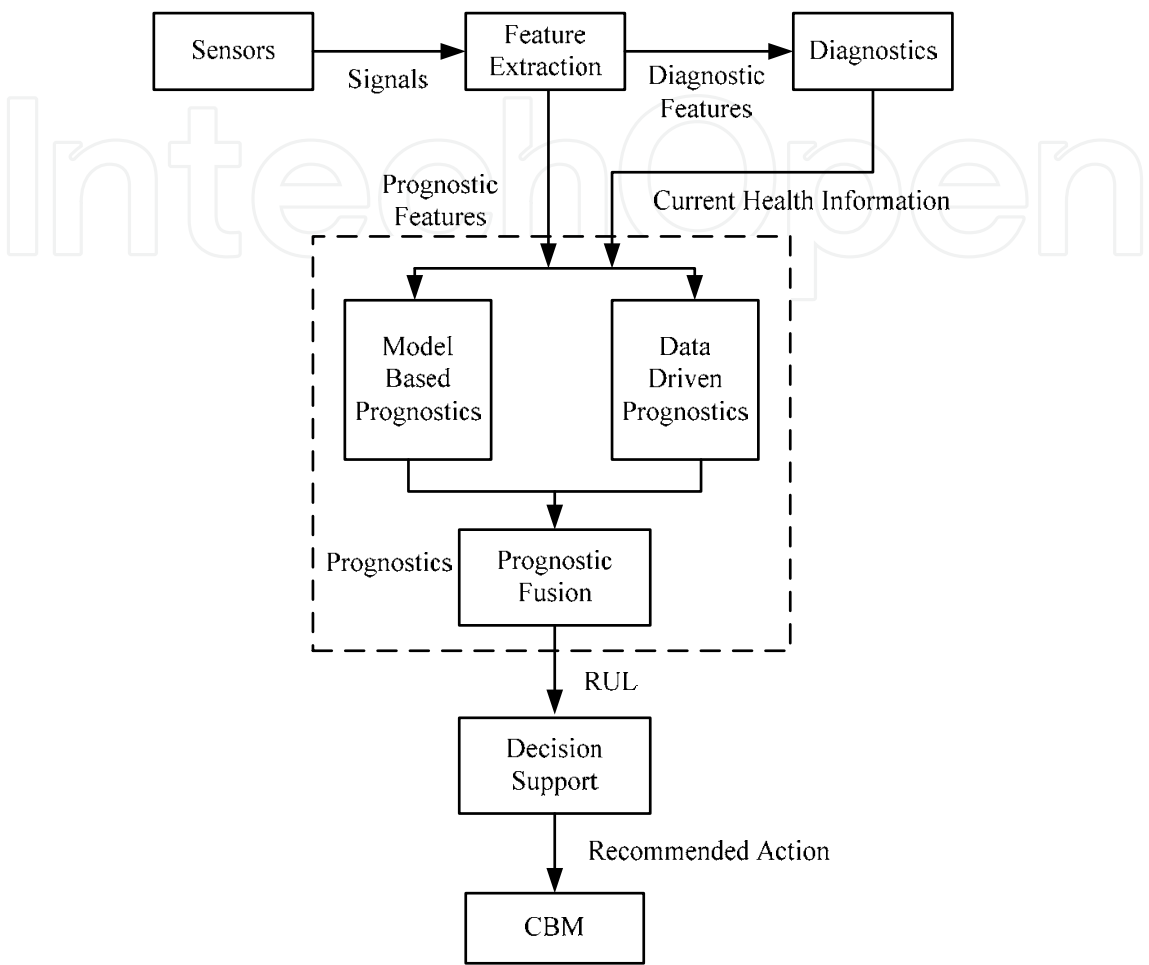
Fig. 29. Functional modules of CBM system

Fault prognostics is the process to project the current health state of equipment into the future taking into account estimates of future usage profiles, thus estimates the remaining useful life (RUL) of machine. The existing prognostic methods can generally be classified as two major categories, namely model based and data driven approaches. Compared to model based approaches, data driven ones do not need the prior knowledge (physical model or domain expert experiences) about system fault condition, thus makes it an effective approach in practical applications. The data-driven approaches are based upon statistical and learning techniques from the theory of pattern recognition.
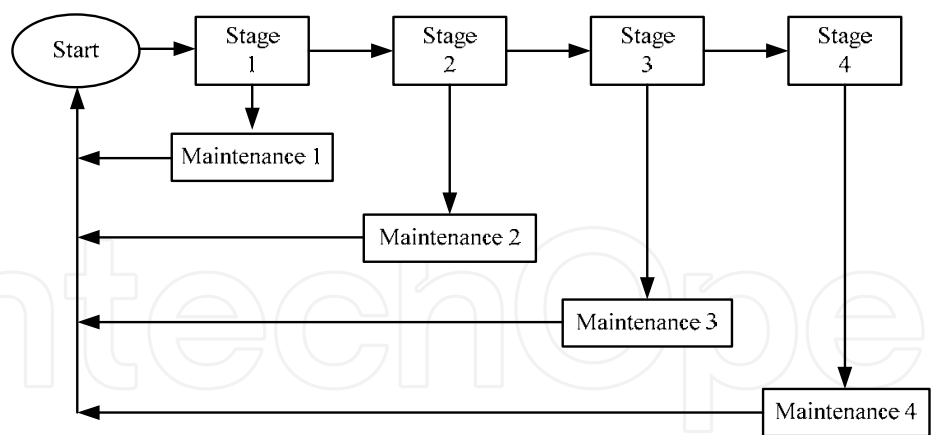
Fig. 30. condition based diagnosis and maintenance methodology

A procedure for diagnosis and condition based maintenance for power transformers is presented in (Setayeshmehr et al. 2004). The condition based diagnosis process uses some of the current diagnosis methods (e.g. Oil test, DGA, PD, etc.) to determine the condition of the transformer. The condition based diagnosis and maintenance methodology is shown in Figure 30 (Setayeshmehr et al. 2004).

Reference (Zhang, Li, Yu and Gao 2007) presents a fault prognostic algorithm based on a generic wavelet neural networks (WNN) architecture whose training process is based on genetic algorithm. The paper used MIMO WNN to conduct modeling task. The structure of wavelet neural networks is shown in Figure 31.
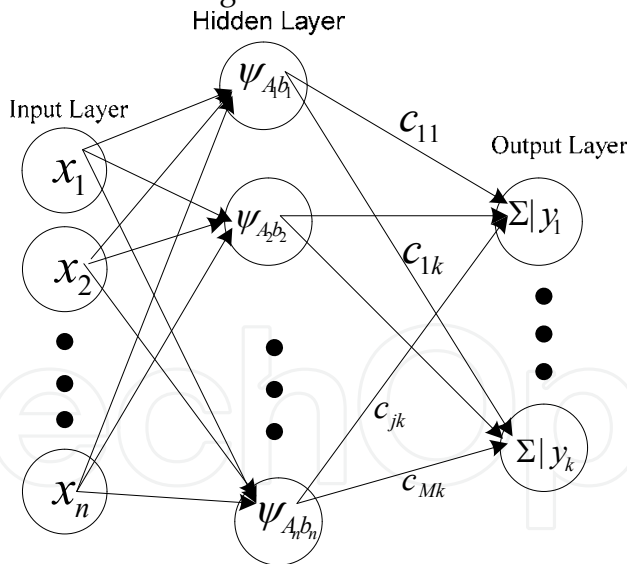

Fig. 31. Structure of wavelet neural networks

A MIMO WNN can be written as:

$$Y = [\Psi_{A_1 b_1}(X) \Psi_{A_2 b_2}(X) \cdots \Psi_{A_M b_M}(X)]C \tag{51}$$

The proposed WNN is employed to learn the input-output relationship using the GA. The training process of WNN includes following 8 procedures:

a. Representation

b. Fitness definition
c. Population initialization
d. Fitness evaluation
e. Selection
f. Crossover
g. Mutation
h. Stopping criteria

4.3 Fault detection application in transformer protection

Power transformers are important devices in an electrical energy system for supplying electricity. In order to obtain a high reliability level from an operation of the power transformer, a precise protection scheme is required. Generally, the transformers can be protected by overcurrent relays, pressure relays and differential relays depending on purposes. For differential protection, the differential current, which is generated by a comparison between the primary current and the secondary current detected via current transformers, is required. The differential protection is aimed at detecting internal faults in transformer windings. In a normal operation or in a fault condition due to the external short circuits, the differential current is relatively small, and the differential relay should not function. However, there are some factors that can cause a needless operation of the differential protection. To avoid the malfunction, the discrimination between internal faults, magnetizing inrush current and external short circuit current is required (Ngaopitakkul et al. 2005).

4.3.1 The method using short time Fourier transforms

A novel approach using the short-time Fourier transform (time frequency analysis tools) for fault detection during impulse testing of power transformers is described in (Al-Ammar et al. 2008). The neutral and/or capacitive transferred currents which are recorded during an impulse test can be directly analyzed with this approach. The primary objective of time-frequency analysis is to be able to define a function that will describe the energy density of a signal simultaneously in time and frequency, and is commonly used in applications to speech, sonar and acoustic signals. Among the few tools, STFT happens to be very common and popular, because the concept behind it is simple yet powerful. The basic idea of STFT is to slice up the signal into suitable overlapping time segments (using windowing methods) and then to Fourier analyse each slice to ascertain the frequencies contained in it. The accumulation of such spectra indicates how the spectrum is varying in time and is called the spectrogram. It is assumed that frequency information is associated with the time index in the middle of each slice of windowed data. STFT of a continuous-time signal $x(t)$ is defined as:

$$STFT(t,\omega) = \int_{-\infty}^{\infty} x(\tau)w(\tau-t)e^{-j\omega\tau}d\tau \qquad (52)$$

where $w(t)$ is the window function and $x(t)$ is the signal to be transformed. $STFT(t,\omega)$ is a complex function representing the phase and magnitude of the signal over time and frequency. The window $w(t)$ is slid along the time domain to establish $STFT(t,\omega)$. In order

to estimate the "local" frequency contents at time , the signal $x(t)$ has to be isolated in the vicinity of time t , and then perform a FFT analysis.

4.3.2 The method using wavelet transforms

Signal processing using wavelet theory has emerged as a powerful tool over the past ten years and has led to significant developments in data analysis, data compression, image and speech processing, multi-resolution analysis etc. The WT like the Fourier transform decomposes a given signal into its frequency components, but differs in providing a non-uniform division of the frequency domain. In addition, unlike the Fourier transform which gives a global representation of the signal, WT provides a local representation in both time and frequency. These results from the fact that the analyzing basis functions in the case of the Fourier transform (namely sines and cosines) extend over infinite time, whereas they are compactly supported functions in the case of WT, thus giving them the localization property. This property greatly facilitates analysis of non-stationary signals, transient detection etc. A mathematical definition of WT follows (Satish 1998):

Let $x(t)$ denote a continuous-time finite energy signal, then WT of $x(t)$ is defined as:

$$WT(a,b) = \int_{-\infty}^{\infty} x(t)g_{(a,b)}(t)dt \tag{53}$$

where

$$g_{(a,b)}(t) = |a|^{(-1/2)} g((t-b)/a) \tag{54}$$

is called the base function or mother wavelet. a , b (real, $a \neq 0$) are the dilation and translation parameters, respectively. A restriction on the choice of $g(t)$ is that it must have a zero average value and be of short duration, which, mathematically, is called the admissibility condition on $g(t)$. Daubechies' wavelet, Morlet wavelet and Harr wavelet are some examples of popularly used functions for $g(t)$.

4.4 Fault detection application in generator protection of Multi-Generator-System

So far the most common generator fault style is stator winding single-phase ground fault, which brings about inter-phase failures and inter-turn faults easily. If the stator ground fault cannot be detected and isolated duly, this fault brings about overheating in the fault point and burns down the stator stick and iron core. So the stator ground fault has very bad influences on the generator normal operating, and we need highly accurate and reliable protection of stator single-phase ground fault to ensure the generator operates safely and reliably. Small or medium power generation systems are Multi-Generator-System (MGS) with more than one generator directly connecting to a bus and operating in parallel commonly. If stator ground fault happened in one of the generators operating in parallel, the generator which have happened single-phase ground fault should be detected and isolated by generator protective relay.

4.4.1 The method based on the grounding leakage current

The scheme utilizing the grounding leakage current of the fundamental component and the third harmonic fault components can detect HIGF. And the faulted generator can be detected and located by comparing the difference of leakage current of the fundamental component and third harmonic fault components between generator neutral and terminal side of each phase.

The features of grounding leakage current can be summarized as follow:

a.   In the faulted generator, the differences of the leakage current variations between the sound and faulted phases are almost equal to the residual current. On the other hand, the differences of the leakage current variations between sound phases are is almost equal to zero.

b.   In the healthy generator, the differences of the leakage current variations between any two phases are also zero under ideal condition.

Hence, protection against generator stator ground fault can be carried out through comparing the differences of leaking current variations. A difference larger than a threshold would indicate the presence of a ground fault.

The operation criterion is:

$$I_d \geq KI_r + I_{d0} \tag{55}$$

Where, K is the restraint coefficient, I_{d0} is the pickup current, I_r represents restraining current, I_d represents the maximum of the difference of the grounding leakage current between phases and it can be calculated:

$$I_d = \max(|\Delta I_{AB}|, |\Delta I_{BC}|, |\Delta I_{CA}|) \tag{56}$$

Under normal conditions, the differences of the grounding leakage current between healthy phases would equal to zero. Considering the influences of the measuring error, the differences of the grounding leakage current between healthy phases would be a small value. The setting value of I_{d0} can be set to the minimum of the differential current between phases which can stands aside, namely $|\Delta I_{BC}|$. If single-phase earthed fault happen in phase A, I_{d0} can be obtained by:

$$I_{d0} = |\Delta i_B(k) - \Delta i_C(k)| = |\Delta i_{BC}| \tag{57}$$

The restraining current I_r can be set to the minimum of the grounding leakage current of three phases, namely the single-phase ground leakage capacitive current.

$$I_r = \min(|\Delta I_A|, |\Delta I_B|, |\Delta I_C|) = 3\omega C_1 \Delta U_3' \tag{58}$$

The generator ground fault current equals the vector sum of the each generator grounding leakage current, the grounding current flowing through the Peterson-coil or resistance of the generator neutral side, and the capacitive current of the external facilities such as external transformers. The restraint coefficient K can be determined based on the neutral grounding modes, compensation factor, and the number of generators operating in parallel. The influence of the Peterson-coil to the third harmonic current is very small. If there are 2 generators operating in parallel, the restraint coefficient K can be set to 1. If there are 3 generators operating in parallel, the restraint coefficient K can be set to 1.5. If there are 4 generators operating in parallel, the restraint coefficient K can be set to 1.8.

Only the grounding leakage current of the fundamental component and third harmonic

component on the neutral and terminal sides of each phase of the generator stator need be measured by the protection scheme. All kinds of single-phase ground fault can be detected with high reliability by the scheme. The scheme has high sensitivity and robustness (Xia et al. 2007).

4.4.2 The method based on the fault resistance measurement

The faulted generator can be detected with the differences of the leakage current. If the difference is larger than a pre-set threshold value, the generator is considered to have a ground fault. Unfortunately, the threshold is difficult to set. In order to improve its performance, a fault-resistance based protection scheme is proposed as follows.

The fault resistance can be calculated from fault voltage and fault current:

$$R_f = \frac{\Delta \dot{U}_0{}'}{\dot{I}_f} = \frac{\Delta \dot{U}_0{}'}{\Delta \dot{I}_{A1} - \Delta \dot{I}_{B1}} \tag{59}$$

To implement the fault-resistant based protection scheme, three phase calculated resistances are defined as:

$$R_{dA} = \left| \frac{\Delta \dot{U}_0}{\Delta \dot{I}_A - (\Delta \dot{I}_B + \Delta \dot{I}_C)/2} \right| \tag{60}$$

$$R_{dB} = \left| \frac{\Delta \dot{U}_0}{\Delta \dot{I}_B - (\Delta \dot{I}_A + \Delta \dot{I}_C)/2} \right| \tag{61}$$

$$R_{dC} = \left| \frac{\Delta \dot{U}_0}{\Delta \dot{I}_C - (\Delta \dot{I}_A + \Delta \dot{I}_B)/2} \right| \tag{62}$$

The generator calculated resistance is defined as:

$$R_d = \min(R_{dA}, R_{dB}, R_{dC}) \tag{63}$$

With these definitions, three phase calculated resistances of the faulted generator are:

$$R_{dA1} = \left| \frac{\Delta \dot{U}_0{}'}{\Delta \dot{I}_{A1} - (\Delta \dot{I}_{B1} + \Delta \dot{I}_{C1})/2} \right| = \left| \frac{\Delta \dot{U}_0{}'}{-\dot{I}_f} \right| = R_f \tag{64}$$

$$R_{dB1} = \left| \frac{\Delta \dot{U}_0{}'}{\Delta \dot{I}_{B1} - (\Delta \dot{I}_{A1} + \Delta \dot{I}_{C1})/2} \right| = \left| \frac{2\Delta \dot{U}_0{}'}{\dot{I}_f} \right| = 2R_f \tag{65}$$

$$R_{dC1} = \left| \frac{\Delta \dot{U}_0{}'}{\Delta \dot{I}_{C1} - (\Delta \dot{I}_{A1} + \Delta \dot{I}_{B1})/2} \right| = \left| \frac{2\Delta \dot{U}_0{}'}{\dot{I}_f} \right| = 2R_f \tag{66}$$

So, the calculated resistance in the faulted generator is:

$$R_{d1} = \min(R_{dA1}, R_{dB1}, R_{dC1}) = R_f \tag{67}$$

The calculated resistance in the normal generator is:

$$R_{d2} = \min(R_{dA2}, R_{dB2}, R_{dC2}) \rightarrow \infty \tag{68}$$

If the calculated resistance is less than its threshold R_{set}, ground fault is deemed to have occurred in the generator stator winding.

To improve protection reliability, two protection criteria are applied. One criterion is low

resistance protection, presented as above. If the calculated resistance is less than its threshold R_{set} , ground fault is deemed to have occurred in the generator stator winding. The threshold R_{set} is usually set from 1kΩ to 8kΩ. The larger the generator capacity, the higher is threshold setting. The other protection criterion is through resistance comparing: the generator in the MGS which has the lowest calculated resistance is the faulted unit.

The protection scheme is shown in Figure 32. It has the following steps:

a. The generator stator currents are monitored in the neutral and on the terminal sides in real time. The neutral point voltage is also monitored. The parameters are sampled by A/D converters.

b. If the zero sequence voltage is larger than its threshold, ground fault is detected, and the above proposed ground fault protection is initiated.

c. The faulted generator is the unit with its calculated resistance values less than its threshold R_{set} , or with the lowest calculated resistance among the units in the MGS.

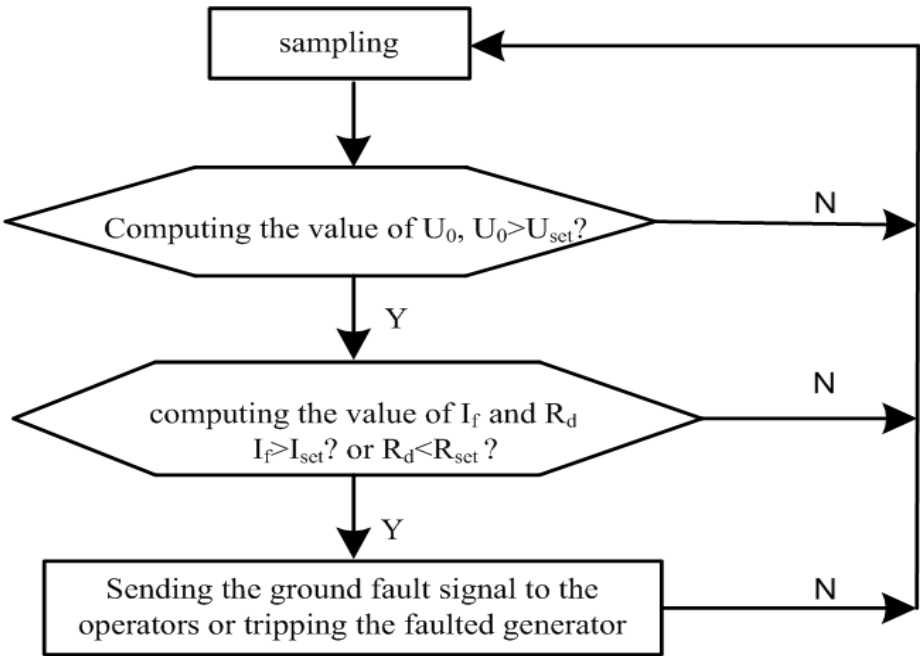d. The signal identifying the unit with the ground fault is sent to operator and the faulted generator is tripped.

Fig. 32. Resistance protection scheme

4.5 Fault detection application in line protection

Grounding faults generate voltage and current traveling wave. They spread from the fault point to power station, and then to other sound feeders. The transmission procedure can be described as Figure 33. The traveling wave will fade down during spreading abroad.
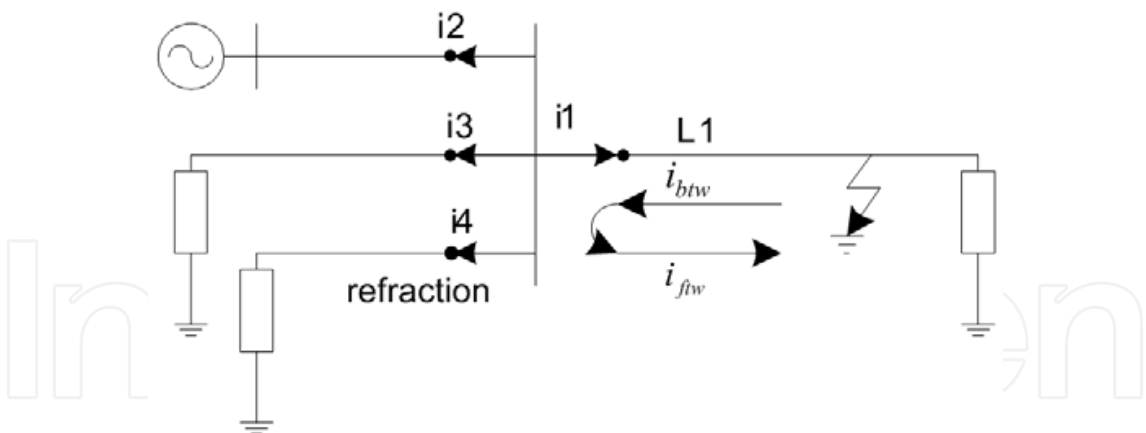
Fig. 33. Fault line selection based on traveling wave current

The reflecting occurs at the point (bus for the example) where impedance does not match. The traveling wave flows in the fault line is the strongest, which is the superposition of the initial inverted traveling wave (i_{btw}) and forward traveling wave (i_{ftw}) whose direction change after reflecting. Whereas the traveling wave in the sound lines is the refraction component of the traveling wave at the fault point and fault lines. So the traveling wave in the sound lines is very small, and its polarity is just reverse to the traveling wave in the fault line.

The traveling wave caused by fault can be detected in each feeder, and the traveling wave in the fault feeder is the largest one. The polarity of traveling wave in the fault feeder is just opposite to the polarity of traveling wave in sound feeders. The fault feeder can thus be detected by comparing the magnitude and polarity of traveling wave caused by distribution system faults in all feeders. The zero sequence components are often used.

Fig. 34. Traveling wave detection device

In order to detect the faults generated traveling wave, two types of traveling wave sensors are developed. They are current traveling wave sensor and voltage traveling wave sensor. The current sensor is a coil with magnetic ring iron core (as shown in Figure 34). A transient voltage suppressor (TVS) and a resistance divider are connected to the output of the coil. The output voltage is controlled to be under 50V. The sensor suppresses power-frequency signals and amplifies high-frequency signals above 10 kHz. It is installed at the grounded

line of capacitive equipment (such as CVT, transformer bushing, wall bushing) to capture the current traveling-waves flowing from the equipment to earth, and the grounded line is passing through the core. This installation does not influence the normal operation of the power system.

The traveling wave based detection method has been tested in laboratory. High impedance faults and arcing faults can be detected with high precision. Not enough traveling wave based fault detectors have applied in power system.

4.6 Fault detection application in ineffectively earthed distribution systems

Reliability and safety are always the two important aspects in the design and operation of industry power systems. Unscheduled outage can create personnel and equipment safety problems, have an adverse environmental impact, and can result in substantial economic losses. Ineffectively earthed systems can limit earth fault current and operate indefinitely with an earth fault on one phase, eliminating the need for an immediate shutdown. Thus many industrial power systems have been operated with floating neutral or high resistance earthed neutral.

The earth fault current in ineffectively earthed systems is usually not more than ten amperes. It is difficult to detect ground faults and isolate the faulted feeder. In order to improve them, some feeder terminal unit (FTU) based ground fault protectors are developed as follow:

4.6.1 Zero sequence overcurrent protection

Figure 35 shows zero sequence current based earth fault detectors (EFD) installed in a small distribution system.
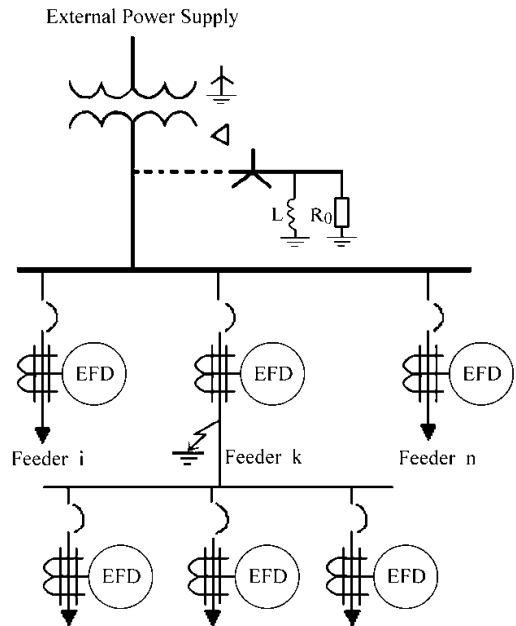

Fig. 35. Zero sequence current based earth fault detectors (EFD) installed in a small distribution system.

If the zero sequence current (I_0) in a feeder is larger than its threshold, this feeder is identified as the ground fault feeder. The threshold of feeder m (I_{0mset}) is usually set as the

magnitude of the capacitive current (I_{cm}) in feeder m caused by other feeder direct earth faults, and it is sure that I, is larger than the least value (I_{0m}) that can be measured accurately by the digital measurement unit (Zeng et al. 2004).

$$I_{0mset} = K_{0m}Max(I_{cm}, I_{0m})$$ (69)

Where, K_{0m} is the reliability coefficient.

The zero sequence current in the faulted feeder k detected by EFD is the sum of charging currents of all other sound feeders (feeder i and n) and the neutral point current. Whereas, in the occurrence of other feeder earth fault the zero sequence current in the sound feeder k is its own capacitive charging currents and its extended feeders (feeders a, b and c). In some cases, the charging capacitive currents in the feeder k and its extended feeders (feeders *a, b* and *c*) are possibly bigger than that in the other feeders. The zero sequence current in feeder k caused by its own earth fault is less than that caused by other feeder earth fault. The zero sequence overcurrent protection is thus difficult to be set.

4.6.2 Negative sequence current protection

In Figure 36 (Zeng et al. 2001), an ineffectively earthed system with n feeders has an earth fault on feeder k. The system is a symmetrical radial network with only one source. When earth fault occurs, the distribution capacitance between the three phases of the system and ground is considered. From Figure 36 (b), the positive sequence current ($\dot{I}_1$), the negative sequence current ($\dot{I}_2$) and the zero sequence current ($\dot{I}_0$) through the fault point are equal to one third of fault current ($\dot{I}_f$).
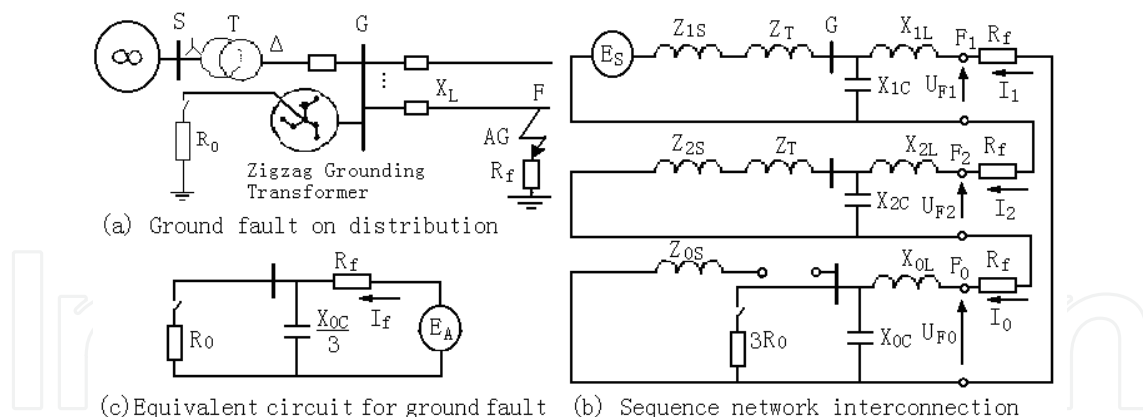

Fig. 36. Sequence network interconnection for "A" phase-to-ground fault

$$\dot{I}_1 = \dot{I}_2 = \dot{I}_0 = \frac{1}{3}\dot{I}_f = \frac{\dot{E}_A}{3R_f + Z_0 + Z_1 + Z_2}$$ (70)

Where: E_A is the faulted phase voltage (supposed fault is in phase A), Z_0 is the zero sequence impedance of this network, Z_1 is the positive sequence impedance, R_f is the fault resistance, and Z_2 is the negative sequence impedance.

Z_1 , Z_2 can be neglected because they are much lower than Z_0 (as Figure 36 (c)), so Eq.70 can be rewritten as:

$$\dot{I}_1 = \dot{I}_2 = \dot{I}_0 = \frac{1}{3}\dot{I}_f = \frac{\dot{E}_A}{3R_f + Z_0} \tag{71}$$

The negative sequence current, generated in the fault point, flows through the whole network, reaches the sources and the loads, and then returns. As the negative sequence impedance of the source Z_{2S} is much lower than that of the loads, most negative sequence current in the fault point flows to the source. Thus the negative sequence current in the earth fault feeder ($\dot{I}_{2k}$) or in the source ($\dot{I}_{2s}$) is approximately equal to one third of the fault current, and it is much larger than that in sound feeder i ($\dot{I}_{2i}$).

$$\left|\dot{I}_{2k}\right| \approx \left|\dot{I}_{2s}\right| \approx \left|\dot{I}_2\right| = \frac{1}{3}\left|\dot{I}_f\right|, \qquad \left|\dot{I}_{2k}\right| >> \left|\dot{I}_{2i}\right| \approx 0 \tag{72}$$

Considering the zero sequence current in the faulted feeder:

$$\dot{I}_{0k} = \frac{1}{3}\dot{I}_f - \dot{I}_{C\,k} \tag{73}$$

Where, $I_{C\,k}$ is the capacitive current in the faulted feeder k .

Comparing Eq.72 and Eq.73, the negative sequence current is usually slightly bigger than the zero sequence current in the faulted feeder.

$$\left|\dot{I}_{2k}\right| \geq \left|\dot{I}_{0k}\right| \tag{74}$$

In sound feeder i , the zero sequence current I_{0i} is approximately equal to its capacitive current I_{ci} . It is usually larger than the negative sequence current, which is approximately zero (Eq.72). Negative sequence current is therefore more sensitive in detecting earth fault feeder than zero sequence current.

Moreover, energy oscillations usually exist in zero sequence circuit between restrikes during arc-grounding fault, but not in negative sequence circuit because the negative sequence impedance of source is so small that energy is quickly faded away after arc extinguishing. Protection schemes based on negative sequence current hence have a better performance in detecting arcing fault than that based on zero sequence current.

The principles for earth fault detection based on negative sequence current are as follow:

a.   Negative Sequence Current Based Overcurrent Protection

If the magnitude of negative sequence current component in a feeder is larger than its threshold, this feeder is identified as the earth fault feeder.

$$\left|\Delta\dot{I}_{2m}\right| > I_{2mset} \tag{75}$$

The threshold of feeder m (I_{2mset}) is usually set as the least value that can be measured accurately by digital measurement unit, and it is sure that I_{2mset} is larger than the magnitude of negative sequence current component in feeder m caused by other feeder directly earth fault.

b.   Difference between Negative Sequence Current and Zero Sequence Current Based Protection

From Eq.74, when the component of negative sequence current is slightly bigger than that of zero sequence current in a feeder, it is identified as the faulted feeder.

$$\left|\Delta \dot{I}_{2m}\right| > K_0 \left|\Delta \dot{I}_{0m}\right| \qquad (76)$$

In order to improve fault detection sensitivity, a reliability coefficient K_0 is used, which is usually set as 0.5.

c.   Negative Sequence Current Based Differential Protection

The component of negative sequence current in the faulty feeder is approximately opposite to that in the source, while that in a sound feeder is approximately equal to zero, and is much lower than that in the source. The faulted feeder can therefore be detected, if the difference between the component of negative sequence current in a feeder and that in the source is smaller than its threshold.

$$\left|\Delta \dot{I}_{2m} + \Delta \dot{I}_{2S}\right| < I_{2msset} \qquad (77)$$

The threshold of feeder m (I_{2msset}) is usually set as a value that is larger than the sum of the magnitudes of negative sequence current component in all sound feeders caused by a directly earth fault of feeder m.

d.   Phase Difference between Negative Sequence Current and Fault Phase Voltage Based Protection

If the phase difference between the negative sequence current in a feeder and the fault phase voltage phasor is near to zero (in same direction), this feeder can be identified as the faulted feeder.

$$\theta_{set1} < \arg(\Delta \dot{I}_{2m}) - \arg(\dot{U}_A) < \theta_{set2} \qquad (78)$$

In order to improve fault detection sensitivity, θ_{set1}, θ_{set2} is usually set as -60^0 and 60^0 respectively.

e.   Fault Point Energy Dissipation Based Protection

If the energy function (in Eq.79) of a feeder is larger than its threshold, this feeder can also be identified as the faulted feeder.

$$W_m(t) = 3\int_{t1}^{t2} u_A \Delta i_{2m} dt > W_{Set} \qquad (79)$$

Where, $t1$ is the time of earth fault initiation, ($t2$-$t1$) is about one cycle (20mS in 50Hz). W_{Set} is usually set as a small positive value.

Among the above fault detection schemes, scheme a, b, c, and e only demand to measure the local current or voltage. These schemes are convenient to be implemented in Remote Terminal Unit (RTU), Feeder Terminal Unit (FTU) and Intelligent Electronic Device (IED) in Distribution Automation (DA) systems.

5. Reference

(2006) Electromagnetic compatibility (EMC)-Part 4-3: Testing and measurement techniques-Radiated, radio-frequency, electromagnetic field immunity test, Third.

Al-Ammar E, Karady GG, Sim HJ (2008) Novel technique to improve the fault detection sensitivity in transformer impulse test. IEEE Transactions on Power Delivery 23:717-725

Amaral JLM, Amaral JFM, Morin D, Tanscheit R (Year) An immune fault detection system with automatic detector generation by genetic algorithms. In: Proceedings of The 7th International Conference on Intelligent Systems Design and Applications, ISDA 2007

Awais MS, S.; Ahmed, N.; Shahid, S. (2003) A comparative study of feed forward neural networks and radial basis neural networks for modeling Tokamak fusion process. Multi Topic Conference, 2003 INMIC 2003 7th International:6

Aydin I, Karakose M, Akin E (Year) Artificial immune inspired fault detection algorithm based on fuzzy clustering and genetic algorithm methods. In: CIMSA 2008 - IEEE Conference on Computational Intelligence for Measurement Systems and Applications Proceedings

Betta G, Liguori C, Pietrosanto A (Year) Use of genetic algorithms for advanced instrument fault detection and isolation schemes. In: Conference Record - IEEE Instrumentation and Measurement Technology Conference

Betta G, Liguori C, Pietrosanto A (1998) An advanced neural-network-based instrument fault detection and isolation scheme. IEEE Transactions on Instrumentation and Measurement 47:507-512

Bittera M, Harťanský R (2006) EM field measurement aspects for electromagnetic compatibility purposes. MEASUREMENT SCIENCE REVIEW 6:14-17

Bossé E, Guitouni A, Valin P (Year) An essay to characterise information fusion systems. In: 2006 9th International Conference on Information Fusion, FUSION

Chen LJ, Tsao TP, Lin YH (2005) New diagnosis approach to epoxy resin transformer partial discharge using acoustic technology. IEEE Transactions on Power Delivery 20:2501-2508

Chow M-y, Yee SO (1991) Methodology for on-line incipient fault detection in single-phase squirrel-cage induction motors using artificial neural networks. IEEE Transactions on Energy Conversion 6:536-545

Cooper JH, South WH, Shimshock JF (Year) FIELD TEST EXPERIENCE AND DIAGNOSTIC TECHNIQUES ON 1200-KV GAS INSULATED SUBSTATION COMPONENTS. In: International Conference on Large High Voltage Electric Systems, Paris, Fr

Curry T, Collins EG, Jr., Selekwa M (Year) Robust fault detection using robust estimation and fuzzy logic. In: Proceedings of the American Control Conference

Curry TD, Collins Jr EG (Year) Robust l1 design of a multivariable PI controller using a real-coded genetic algorithm. In: Proceedings of the American Control Conference

Dixon DS, Dutcher C (Year) Feasibility of conducting unit level EMI tests in a system level environment. In: IEEE International Symposium on Electromagnetic Compatibility, Washington, DC, USA

Guo F (2007) Deep Research on both-terminal travelling wave fault location. Shandong University Master's Thesis, Ji Nan, Shandong University, China:34-37

Hartog A (1995) Distributed fibre-optic temperature sensors: technology and applications in the power industry. Power Engineering Journal 9:114-120

Hauptmann P, Hoppe N, Puettmer A (Year) Ultrasonic sensors for process industry. In: Proceedings of the IEEE Ultrasonics Symposium, Atlanta, GA

Jingchao Y, Xianggen Y, Deshu C, Ze Z (Year) Study on the Operating Characteristic of Sampled Value Differential Protection. In: Canadian Conference on Electrical and Computer Engineering

Lippmann RP (1987) INTRODUCTION TO COMPUTING WITH NEURAL NETS. IEEE ASSP magazine 4:4-22

Li T, Zhao Y, Li N, Fen G, H. G (2005) A new method for power quality detection based on HHT. Proceedings of CSEE, China 25:52-56

Liu Z, Zhou JZ, Zou M (Year) Condition based maintenance system of hydroelectric generating unit. In: Proceedings of the IEEE International Conference on Industrial Technology

Middelkoop R (1991) Time-domain calibration of field sensors for electromagnetic pulse (EMP) measurements. IEEE Transactions on Instrumentation and Measurement 40:455-459

Nakamura Y (2008) Noncontact sensor. Patent No:US 7,330,033 B2

Ngaopitakkul A, Kunakorn A, Ngamroo I (Year) Discrimination between external short circuits and internal faults in transformer windings using discrete wavelet transforms. In: Conference Record - IAS Annual Meeting (IEEE Industry Applications Society)

Satish L (1998) Short-time Fourier and wavelet transforms for fault detection in power transformers during impulse tests. IEE Proceedings: Science, Measurement and Technology 145:77-84

Setayeshmehr A, Akbari A, Borsi H, Gockenbach E (Year) A procedure for diagnosis and condition based maintenance for power transformers. In: Conference Record of IEEE International Symposium on Electrical Insulation

Sreedhar R, Fernandez B, Masada GY (Year) Neural network based adaptive fault detection scheme. In: Proceedings of the American Control Conference

Srivani SG, Vittal KP (Year) On line fault detection and an adaptive algorithm to fast distance relaying. In: 2008 Joint International Conference on Power System Technology POWERCON and IEEE Power India Conference, POWERCON 2008

Vemuri AT, Polycarpou MM, Diakourtis SA (1998) Neural network based fault detection in robotic manipulators. IEEE Transactions on Robotics and Automation 14:342-348

Wang X, Qian Q, Chen W (Year) Analyzing fault-induced transients with wavelets. In: Proceedings of the IEEE Power Engineering Society Transmission and Distribution Conference, Chicago, IL

Wang Y, Zeng X, Ma H, Xia Y, Xu Y (Year) Grounding fault protection with sampling value difference in ineffectively earthed power systems. In: 2006 International Conference on Power System Technology, POWERCON2006

Wang Y, Zeng X, Su S (Year) Grounding fault protection with phase current difference for ineffectively earthed power systems. In: Conference Record - IAS Annual Meeting (IEEE Industry Applications Society)

Widrow B, Winter R (1988) NEURAL NETS FOR ADAPTIVE FILTERING AND ADAPTIVE PATTERN RECOGNITION. Computer 21:25-39

Xia Y, Zeng X, Wang Y, Ma H (Year) Stator winding grounding fault protection with third harmonic current difference for multi-generator systems. In: Conference Record - IAS Annual Meeting (IEEE Industry Applications Society)

Xiao'an Q, Xiangjun Z, Xiaoli Z, Zewen L (Year) Traveling wave based distribution lines fault location using Hilbert-Huang Transform. In: Conference Record - IAS Annual Meeting (IEEE Industry Applications Society), Edmonton, AB

Yang JC, Yin XG, Chen DS, Zhang Z, Wang ZH (Year) The Study of Sampled Value Differential Protection. In: Proceedings of the IEEE Power Engineering Society Transmission and Distribution Conference

Zeng X, Guo Z, Su S (Year) Ground fault protection for ineffectively earthed power systems. In: 2004 International Conference on Power System Technology, POWERCON 2004

Zeng X, Li KK, Chan WL, Su S, Wang Y (2008) Ground-fault feeder detection with fault-current and fault-resistance measurement in mine power systems. IEEE Transactions on Industry Applications 44:424-429

Zeng X, Li KK, Chan WL, Yin X (Year) Novel techniques for earth fault feeder detection based on negative sequence current in industry power systems. In: Conference Record - IAS Annual Meeting (IEEE Industry Applications Society), Chicago, IL

Zeng X, Xia Y, Ma H, Wang Y (Year) Grounding faulted feeder detection methods applied in Chinese ineffectively earthed distribution systems. In: Conference Record - IAS Annual Meeting (IEEE Industry Applications Society), New Orleans, LA

Zeng X (2000) Reasearch on advanced principles of power lines fault detection & fault location and their implementing with information fusion. Doctoral Dissertation, Wuhan, Huazhong University of science & technology, China 19-21.

Zeng X (2003)On-Site Safety Evaluation for Earth Fault in Mining Power Systems.IEEE TRANSACTIONS ON INDUSTRY APPLICATIONS, 39(6): 1563-1569

Zhang L, Li X, Yu J, Gao Z (Year) A genetic training algorithm of wavelet neural networks for fault prognostics in condition based maintenance. In: 2007 8th International Conference on Electronic Measurement and Instruments, ICEMI

Zhang Y, Lee SR, Zhao H, Wang B, Bingqing L (Year) Research on wavelet analysis in fault signal processing. In: International Conference on Signal Processing Proceedings, ICSP, Beijing

Fault Detection

Edited by Wei Zhang

In this book, a number of innovative fault diagnosis algorithms in recently years are introduced. These methods can detect failures of various types of system effectively, and with a relatively high significance.

How to reference

In order to correctly reference this scholarly work, feel free to copy and paste the following:

Zeng Xiangjun,Wang Yuanyuan and Xu Yao (2010). Faults Detection for Power Systems, Fault Detection, Wei Zhang (Ed.), ISBN: 978-953-307-037-7, InTech, Available from: http://www.intechopen.com/books/fault-detection/faults-detection-for-power-systems

INTECH
open science | open minds